NASA CONTRACTOR REPORT

NASA CR-1089

SEMICONDUCTOR PIEZOJUNCTION TRANSDUCERS

by J. J. Wortman

Prepared by
RESEARCH TRIANGLE INSTITUTE
Research Triangle Park, N. C.
for

NATIONAL AERONAUTICS AND SPACE ADMINISTRATION • WASHINGTON, D. C. • JUNE 1968

NASA CR-1089

Jun 68

SEMICONDUCTOR PIEZOJUNCTION TRANSDUCERS

By J. J. Wortman

Prepared under Contract No. NASr-222 by
RESEARCH TRIANGLE INSTITUTE
Research Triangle Park, N.C.

for

NATIONAL AERONAUTICS AND SPACE ADMINISTRATION

For sale by the Clearinghouse for Federal Scientific and Technical Information
Springfield, Virginia 22151 – CFSTI price $3.00

FOREWORD

This report was prepared by the Research Triangle Institute, Research Triangle Park, North Carolina, on NASA Contract NASr-222, "Feasibility Study of Piezotransistor Accelerometer". This work was administered under the directions of the Instrument Research Division at Langley Research Center by Mr. John Olivero and Mr. Charles Hardesty and of the Office of Advanced Research and Technology Division at NASA Headquarters by Dr. Wolfgang Menzel.

This study began in June 1964 and was concluded in October 1966. The present report covers the period from September 1965 to October 1966. It was performed by the Solid State Laboratory of the Research Triangle Institute under the general direction of Dr. R. M. Burger. While Dr. J. J. Wortman was the project engineer, the entire technical staff has participated to some degree in this effort. Specific credits are due Dr. J. R. Hauser, P. P. Rasberry, R. R. Stockard, H. L. Honbarrier and A. D. Brooks for their invaluable contribution to this investigation. Thanks are also due Mr. T. O. Finley at the Langley Research Center for his aid in testing the accelerometers.

ABSTRACT

Techniques for utilizing the piezojunction effect as the sensory element in transducers are discussed. A new technique for applying the pheonomenon (silicon needle) in a broad class of mechanical transducers has been developed and demonstrated in several transducers. Particular emphasis was placed on accelerometers where it was shown that devices could be fabricated with resonant frequencies greater than 3 KC, capable of measuring ac and dc accelerations in the range from ± 1 g to ± 100 g.

Several techniques were developed for providing a digital output for the piezojunction sensors.

CONTENTS

LIST OF FIGURES

LIST OF FIGURES (continued)

LIST OF FIGURES (continued)

Section I

INTRODUCTION AND DISCUSSION

The purpose of this study has been to determine the feasibility of utilizing the piezojunction effect as the sensory phenomenon in accelerometers and other transducers. The present report is concerned primarily with application of the piezojunction effect. The results of a study of the physics and an analytical description of the phenomena has already been reported in NASA CR-275 (hereafter referred to as I).

Since the discovery that mechanical strain could induce large reversible changes in the electrical properties of p-n junctions (piezojunction effect), there has been much interest in the phenomenon for possible use in mechanical transducers.[2-3] A variety of techniques have been used to induce the effect in p-n junction structures and to observe the phenomenon. The most common experiments have consisted of applying mechanical force into or near the junction region of diodes and transistors by means of a diamond or steel indenter point. Changes in the electrical properties of the device under stress are typically observed by holding the applied voltage constant and observing changes in the device current. For example, a one gram load applied to an ordinary diamond phonograph needle (radius of curvature of approximately 1 mil) in contact with the junction of a diode can cause orders of magnitude changes in diode current. Indenter points are used because one of the requirements for producing the piezojunction effect is large anisotropic stresses, greater than 10^9 dynes/cm^2.

Several factors make the piezojunction phenomena particularly attractive as the sensory element in mechanical transducers: (1) the effect is solid state and as such is compatible with modern solid state techniques;

(2) the sensing element is ultra-small in size and weight and requires low power (3) it is sensitive; (4) it represents a possible increase in resonant frequency of an order of magnitude or greater over present devices; and (5) it responds to both static and dynamic stimuli. Perhaps the most unattractive feature is that a new technology is needed for the fabrication and application of such sensors in practical applications. For example, the stress levels required to induce the effect are near the fracture strength of the semiconductor, which means that good creative designs will be required in practical applications to prevent overstress and destruction of the devices.

Several physical mechanisms have been proposed as the underlying mechanism responsible for the effect: (1) stress induced changes in generation-recombination centers,[4-5] (2) changes in lifetime[6-7] and (3) changes in energy band structures.[1,8,9] The model first proposed for the effect was based on the reversible creation and relieving of generation-recombination centers in the semiconducting material. Closely related to this model is one that postulates a stress induced change in carrier lifetime. Neither of these models are adequate to explain the many facets of the observed phenomenon. A model based on stress induced changes in the energy band structure of the material has been used to explain most of the observations which are reversible. The piezojunction effect is complex in nature and in many cases probably involves each of the above mentioned mechanisms.

The theoretical model of the phenomenon based on stress induced changes in the energy band structure is treated in detail in Ref. 1 . In general in extrinsic material, this model neglects any effects of stress on any junction parameters except the minority carrier concentration.

The intrinsic carrier concentration is given by

$$n_i^2 = pn = n_{io}^2 \gamma_\nu(\sigma), \tag{1.1}$$

where pn is the product of the electron and hole concentration, n_{io} is the unstressed intrinsic carrier concentration, and $\gamma_\nu(\sigma)$ is the factor that accounts for the stress state. The (σ) is used to show a functional stress, σ, dependence. The factor $\gamma_\nu(\sigma)$ accounts for the effects of stress on the multivalley nature of silicon and germanium, for example, as well as crystal orientation and doping level. As shown in I for stress levels above 10^9 dynes/cm^2, $\gamma_\nu(\sigma)$ can usually be approximated by

$$\gamma_\nu(\sigma) = C_1 e^{C_2\sigma} \tag{1.2}$$

where C_1 and C_2 are constants depending on the material and crystallographic orientation.

The electronic current flowing across a p-n junction can be broken into two parts: (1) that resulting from diffusion (Shockley or Ideal) current, and (2) that resulting from generation-recombination in the junction. The total current for a forward biased junction is

$$I = I_{01} \gamma_\nu(\sigma) e^{qV/kT} + I_{02} \sqrt{\gamma_\nu(\sigma)} e^{qV/2kT}, \tag{1.3}$$

where I_{01} and I_{02} are constants depending on the junction parameters and V is the applied voltage. The second term is the current resulting from generation-recombination. Note that the latter current is not as stress sensitive as the diffusion current since it is multiplied by $\sqrt{\gamma_\nu(\sigma)}$. In the reverse biased mode the total current is

$$I = I_{01}\gamma_\nu(\sigma) + I_{03}\sqrt{\gamma_\nu(\sigma)} \quad (V + V_0)^{1/2} \tag{1.4}$$

where V_0 is the junction built in potential and I_{03} is a constant.

Figure 1.1 shows the forward biased characteristics of a silicon mesa diode for several stress levels. The stress was applied by means of a steel post forced against the diode mesa of 33 microns in diameter. The solid curve is a theoretical curve using Eq. (1.3)

The breakdown voltage of p-n junctions is also stress sensitive.[8,10,11] The sensitivity of the breakdown voltage is much less than the diode current. The relative change in breakdown voltage $(\Delta V/V_B)$ in silicon is

$$\frac{\Delta V}{V_B} = -(10^{-12}\ \text{cm}^2/\text{dyne})\sigma\ , \tag{1.5}$$

where σ is the magnitude of the applied stress. The crystal orientation is not important in stress effects on breakdown voltage in silicon. In germanium, however, the effect is much more complicated.[8]

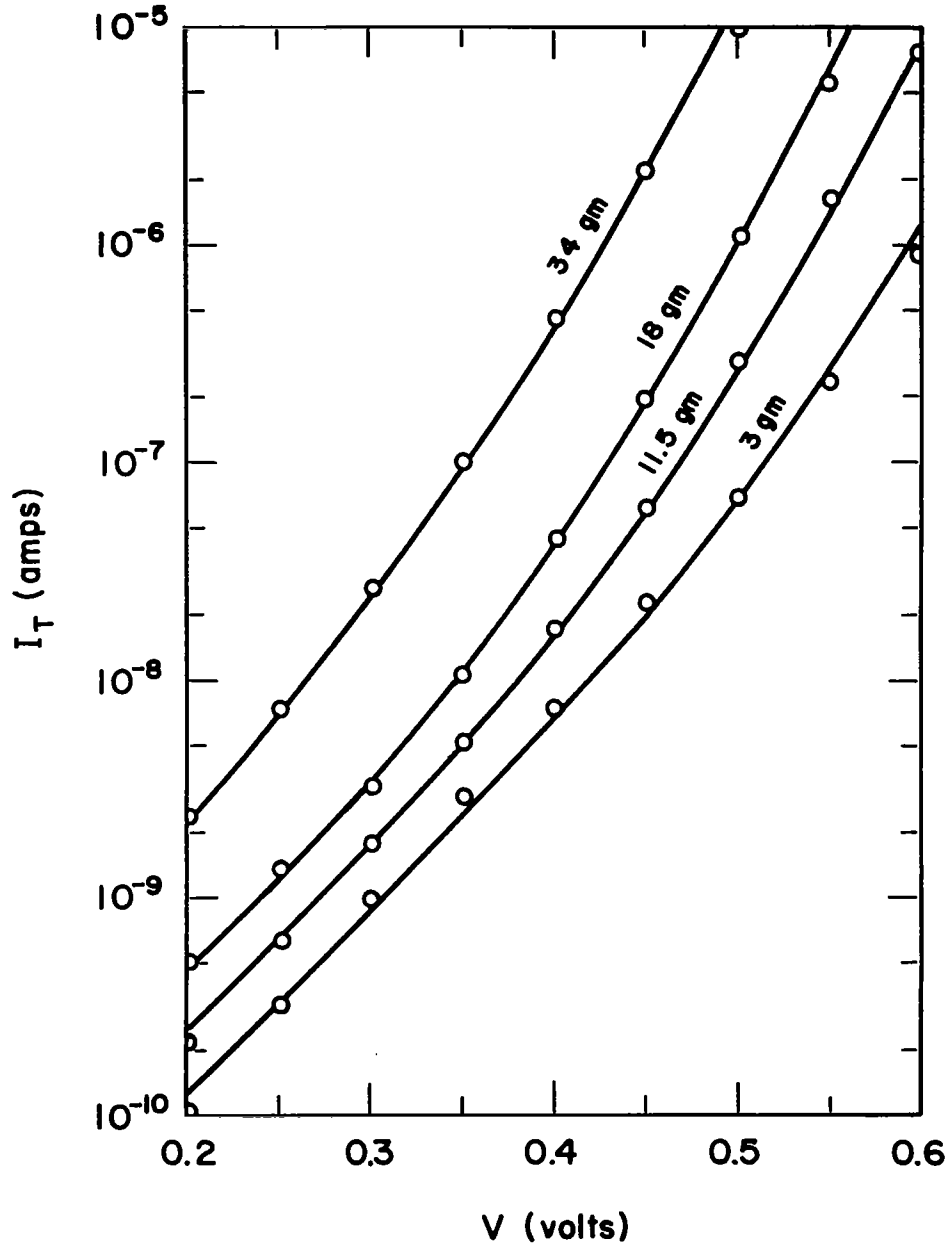

Figure 1.1 Forward Biased I-V characteristics of a mesa diode subjected to stress. (The applied force is shown.)

Section II

STRESS COUPLING TECHNIQUES

2.1 Introduction

In order to utilize p-n junction devices as stress transducers the stress level must be on the order of 10^9 - 10^{10} dynes/cm^2. These stress levels are near the fracture strength of silicon and germanium. The fracture strength as measured using silicon bars is on the order of 3×10^9 dynes/cm^2. This value might be considered as a bulk value and, as evidenced by the stress levels used in this work, and the work of others, the fracture strength over small regions is considerably larger ($\sim 3 \times 10^{10}$ dynes/cm^2). Any useful transducer which utilizes the piezojunction effect must be designed with this fracture strength in mind.

There are several methods of obtaining the high stress levels needed for the piezojunction effect. Some of these methods are discussed in the following sections. Particular emphasis has been placed on the semiconductor needle due to its potential usefulness.

2.2 Indenter Point

The first and most widely used method of applying stress to p-n junction devices in early piezojunction experiments and transducers has been with indenter points. An indenter point, in most cases, is simply a steel, diamond, or sapphire phonograph needle. Stress is applied to a p-n junction device by first placing the indenter point on the junction to be stressed and then applying a calibrated force to the indenter.

The major advantage to using an indenter point is that the stress is not a linear function of the applied force and only a small portion of the total sample is stressed. As force is increased the stressed area increases. This means that fracture due to overstressing is less likely to occur. The most serious disadvantage inherent in this method of stress application is the difficulty of aligning the indenter point and the small junction area so that the point makes contact to the desired location on the junction. Since the stress levels required to produce the piezojunction phenomenon are high, it is necessary that the stressed area be small ($\sim mils^2$) in order that the force required to generate these stress levels is not mammoth. The alignment process is very tedious and must be performed with the aid of a microscope. The complexity of this process is magnified several times when the indentor point stressing method is used in workable transducers which must be subjected to other than laboratory environments. Any lateral movement of the indenter point removes it from the desired junction area and often causes permanent damage to the junction.

Another disadvantage of the indenter point method of stress application is the difficulty of determining the area over which the stressing force is applied. This area, along with applied force, must be known in order to accurately predict the applied stress.

The indenter point method of stressing has been used successfully to build laboratory transducers for accelerometers[12]. Reference 12 describes in some detail the methods used and the results obtained using the indenter point method.

A variation of the indenter point method is often used to apply stress to mesa devices. The indenter point is called a post in this instance because the radius of curvature of the indenter point is much larger than the diameter of the device being stressed. Thus, the entire area of the junction device is stressed by the post. Alignment in this case is not as critical and difficult. Mesa devices are, however, more susceptable to environmental effects and also electrical contact can be a problem. This approach could prove to be a useful technique, particularly if more than one device is stressed at one time with the same post.

2.3 Cantilever Beam

A cantilever beam can be used to apply stress to a p-n junction. This can be accomplished by first fabricating a small, thin beam from single-crystal silicon. A p-n junction is then formed on one side of the beam. Stress is applied by forcing the loose end of the beam up or down. The big disadvantage to such a system is the fracture strength of silicon. In general, a cantilever beam will fracture due to bulk imperfections before the stress levels necessary to effect p-n junction characteristics are reached. Attempts have been made to solve this problem by etching a notch in the beam directly opposite the junction[13]. Although this method of concentrating the stress has had some success, the manufacturing processes and yield will likely prohibit its use. Also, it would be very fragile and easy to overstress.

A variation of the cantilever beam is a beam which is attached to a fixed base at both ends. The principle of operation is identical to the cantilever beam except force is applied to the center of the beam.

The advantages of these methods over the indenter point and post methods is that no alignment problem exists. Also, electrical contact with all junctions is easily attained.

2.4 Diaphragm

Another method of utilizing the piezojunction phenomenon is a semiconductor diaphragm. The diaphragm is etched from a substrate of the desired material to a thickness at which a reasonable force will create the desired stress level. For silicon reasonable forces leads to a thickness less than 5 mils. Here the p-n junction is formed in the center of the diaphragm. It is preferable to use the planar process for this junction formation. Stress is applied to the junction in the same manner as for the cantilever beam.

This diaphragm is extremely fragile and, thus, very difficult to fabricate. However, it shows a great potential for application to pressure transducers.

2.5 Bonded Chip

One of the major disadvantages of any technique for applying the stress which depends for its operation on stressing large volumes of the semiconductor sample is the limited fracture strength which places the weakest point in the system in the position of controlling the upper limit on stress level. One way to avoid this problem is to bond a thin semiconductor chip onto a beam of some material other than silicon. The bond between the beam and the chip must transmit the stress. If the beam is much thicker than the chip then as the beam is stressed the ultimate

mechanical properties are set by the beam and not the chip. In this manner one may avoid an unstable mechanical system if the chip is thin enough so that it does not influence the stress in the beam. If the semiconductor sample does fracture, it may not be near the junction and the device could remain operative.

The problem here is the bond. Two techniques come to mind (1) eutectic bonding utilizing the gold silicon eutectic similar to that used in bonding chips to headers in transistor technology and (2) epoxy. In each of these techniques, the chip must be thin in order to reduce the stress on the bond.

2.6 Semiconductor Needle Sensor

The last method to be discussed for the application of stress to a junction device, and the method considered most applicable to transducers, is the semiconductor needle as shown in Fig. 2-1. The semiconductor needle is an outgrowth of alignment difficulties encountered with the indenter point stressing method. A semiconductor needle is fabricated from a bar of the desired material by using an electroetching technique developed for this purpose. A p-n junction is formed on the apex of the needle by either the mesa or planar techniques, and stress is applied by forcing the needle onto a conductive surface.

The needle sensor is formed by: (1) fabricating the desired silicon blank (rectangular rod), (2) cleaning the blank, (3) electro-etching a conically shaped point on the blank, (4) cleaning, and (5) forming the p-n junction or junctions on the apex of the needle.

2.7 Needle Fabrication Method

The first step in the needle fabrication process is to form the needle blank. The blank is a rectangular bar of silicon approximately 1/2 inch long and 20 mils on each side. The dimensions of the bar are not important with the exception that the sides must be very nearly equal (square perpendicular to the axis). If the rod is not square to within 1/2 mil on each side, the resulting needle tip will be wedge shaped and not conical as desired. A round rod is more desirable than a square rod, however, experiments have shown that the square bars are acceptable.

A cleaning process similar to that used commercially in the production of semiconductor devices was modified and used to clean the silicon starting blanks in order to insure proper etching. The purpose of this

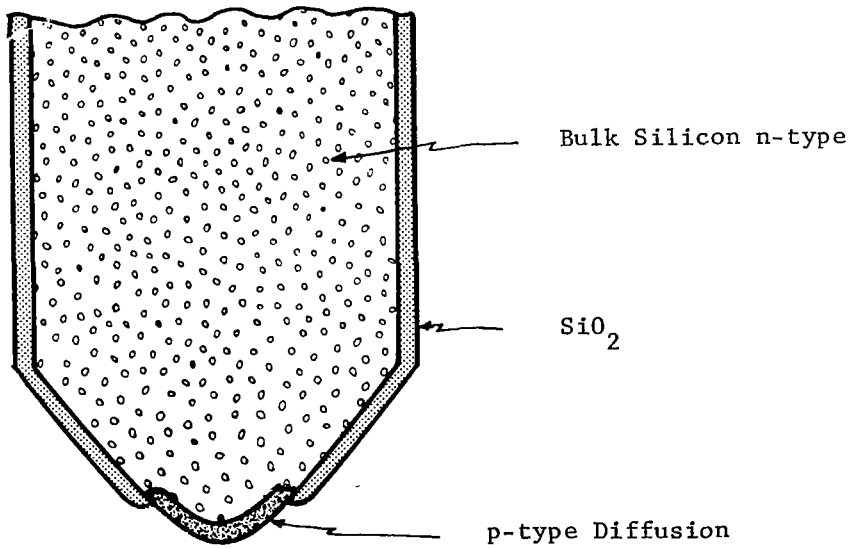

Fig. 2-1. A Sketch of the Silicon Needle Diode Sensor.

is to thoroughly remove all contaminants from the surface of the silicon, including any that might have been introduced during the mechanical slicing operation.

The next step in the needle formation process is the electrochemical etching of the needle tip. This was done by slowly lowering and raising one end of the needle blank into an etch solution. An electric potential (a.c.) was maintained between the needle blank and an electrode in the etch solution. A motor driven apparatus was designed and assembled which controlled the amount of time the starting bar remained in the etching solution and the depth to which it is submerged. It is desirable that this depth be as shallow as possible in order that the mechanical strength of the final needle be maximized. The shallowest depth practical was found to be approximately 1/8 of an inch. The silicon bar was submerged into and retrieved from the etching solution by a piston driven by the motor through a lever arm. A photograph of the apparatus is shown in Fig. 2-2.

The solution used to etch the rectangular silicon bars into needles was composed of a mixture of concentrated HNO_3 and concentrated HF. The mixture ratio was defined as volume of HNO_3 divided by volume of HF and was varied from a high of 14 to a low of 3.5 in an effort to determine its effect on the completed needle. Simultaneously, the electroetching current was varied from 20 ma to 70 ma. The purpose of this procedure was to obtain a balance between chemical and electrical etching phenomena. It was determined that a mixture ratio above 7 was not sufficient to provide a proper chemical contribution to the etching process while a ratio below 4.5 provided an excessive chemical contribution. A low ratio caused an "orange

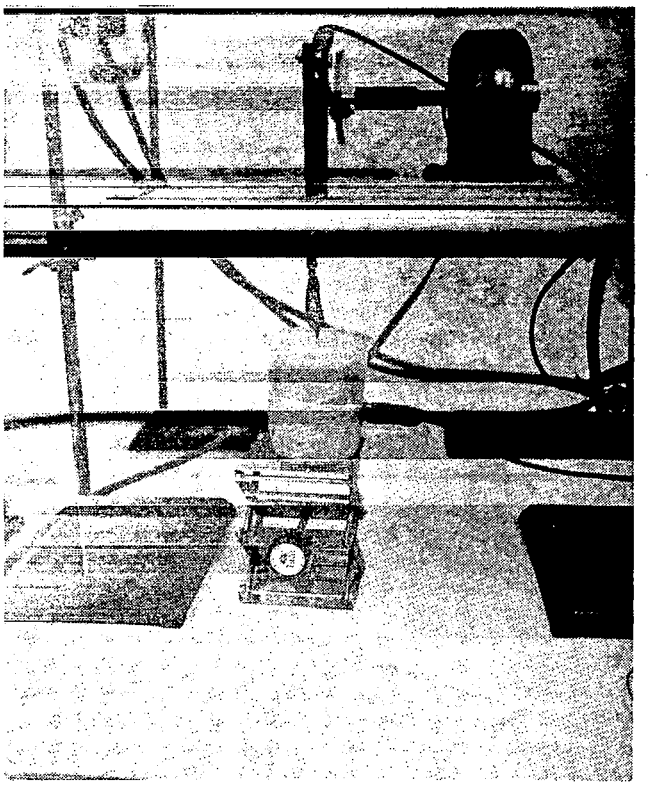

Fig. 2-2. Photograph of the Apparatus Used to Etch the Silicon Bars Into Needles.

peel" effect on the surface of the needle tip and caused the cone of the needle to have an uneven profile. An example of an excessively low mixture ratio is shown in Fig. 2-3. A high mixture ratio resulted in blunt tips because etching action was not sufficient to effectively sharpen the silicon. An example of a high ratio is shown in Fig. 2-4.

When the mixture ratio was outside the prescribed bounds, a proper balance could not be attained by manipulating the current level. A current level above approximately 60 ma increased the electrical contribution to a point of unattainable equillibrium while current below 20 ma resulted in an unbalance in favor of chemical etching. The optimum mixture ratio-current combination was found to be approximately 4.7 at

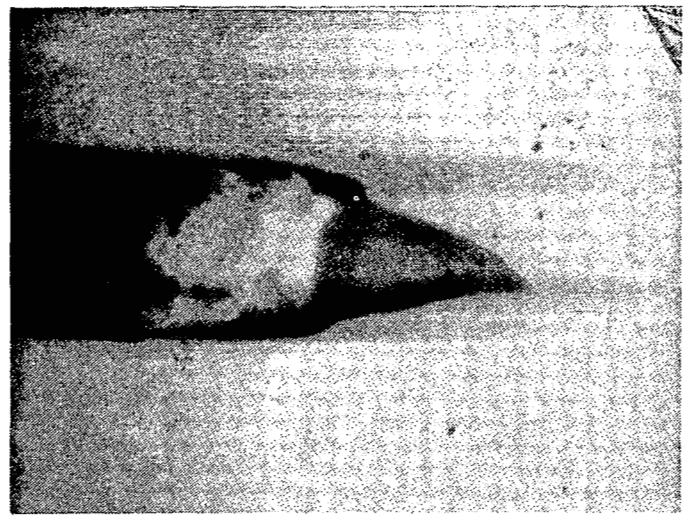

Fig. 2-3. Photomicrograph of a Silicon Needle - Low Mixture Ratio (1 Ω-cm n-type silicon).

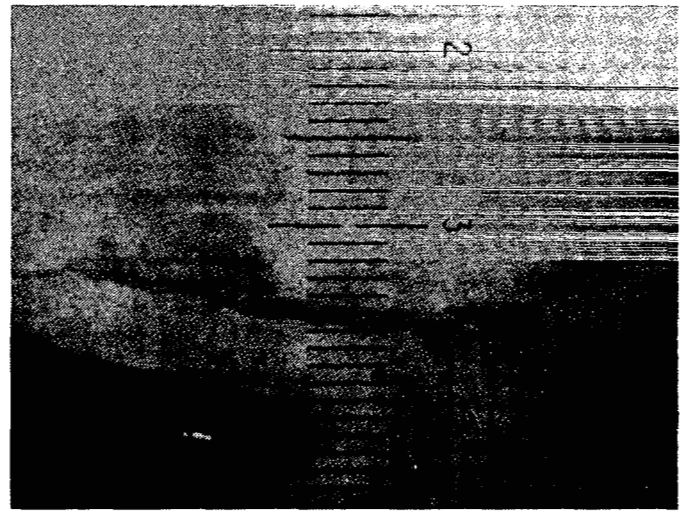

Fig. 2-4. Photomicrograph of a Silicon Needle - High Mixture Ratio (1 Ω-cm n-type silicon).

50 ma. However, the current level did not have nearly as much affect on the needle as did the mixture ratio.

Also worthy of note is the manner in which the solution was mixed and which had a significant effect on the resultant needle. A non-uniformly mixed solution produced needles of various uncontrollable geometries with all other parameters fixed. This problem was alleviated by agitating the mixture for a period of 10 to 15 minutes before the electroetching process was initiated.

The parameters of time and dip-rate were found to be equally as important as the mixture ratio and current parameters. The dip-rate parameter is the rate at which the silicon blank is lowered into and withdrawn from the etching solution. The time parameter is the elapsed time from the beginning to the end of the dipping process. An excessively short time provided insufficient etching and left the needle with a concave cone and a blunt tip. An excessively long time provided excessive etching and left the needle with a convex cone and a blunt tip. The optimum time was found to be approximately 4 minutes. An example of excessive time is depicted by the needle tip in the photomicrograph of Fig. 2-5 while the effect of insufficient time can be seen in Fig. 2-6.

The dip-rate was found to have a detrimental affect on the finished needle only if this rate was very low. At low dip rates, an "orange peel" effect was present on the surface of the etched portion of the needle. This was attributed to chemical etching during the up portion of the dip rate cycle. Chemical etching was caused by the fact that some residual solution was withdrawn along with the needle, and at low dip-rates, had sufficient time to react while the needle was out of

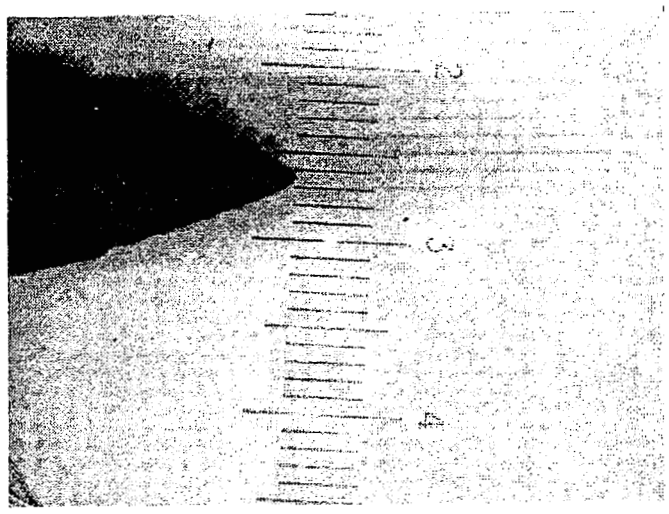

Fig. 2-5. Photomicrograph of 1 Ω-cm n-type Silicon Needle - Etching Time 6 min. (each division is .04 mm).

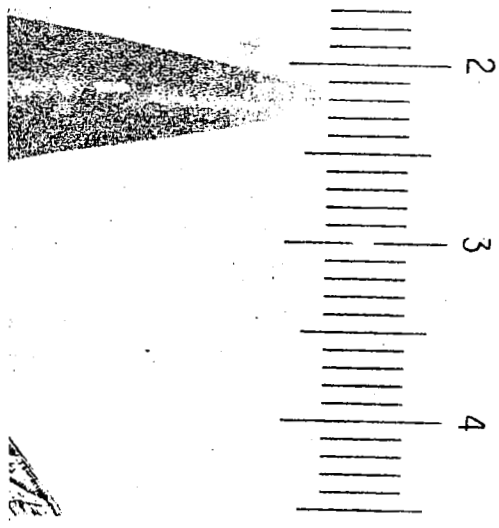

Fig. 2-6. Photomicrograph of 1 Ω-cm n-type Silicon Needle - Etching Time 3 min. (each division is .04 mm).

the solution. Since the needle was out of the solution and thus no current could flow, the etching action was all chemical during this portion of the cycle. The "orange peel" effect was eliminated by increasing the dip-rate to approximately 20 cycles per minute.

The influence of the various parameters such as mixture ratio, etching current, time and dip-rate on the final needle are summarized in Table I. Table I was obtained for 1 ohm-cm n-type silicon. However, the only parameter appreciably affected by a change in resistivity is the current level. A higher current is required for lower resistivities material and vice versa. No appreciable effect has been noted for a change from n to p-type silicon. For very high resistivity starting blanks, an ultraviolet light source aids the etching process.

Using the results of these experiments, it has been possible to reproducibly fabricate silicon needles with approximately the desired geometrical properties. The radii of curvature, as well as tip lengths and surface characteristics, can be controlled to the necessary tolerances. Two needles made using the optimum parameters of Table I are shown in the photomicrographs of Fig. 2-7. It should be noted that the motor driven apparatus is capable of etching any number of needles simultaneously.

2.8 Junction Formation

Once the needle fabrication process was perfected, the next logical step in the development of improved needle sensors was the junction fabrication process. An effort was made to control the parameters of this process with primary emphasis on the method of junction area definition.

Table I

Influence of Electroetching Parameters on Silicon Needle Fabrication

Mixture Ratio	Current (ma)	Time (min)	Dip-Rate (cpm)	Material	Resistivity (Ω - cm)	Remarks
14	70	3	7.7	n-Si	1	Insufficient etching
14	70	3.5	7.7	n-Si	1	Smooth surface, rough concave profile
14	70	4.0	7.7	n-Si	1	Same as above
9.3	70	3.0	7.7	n-Si	1	Rough profile, smooth surface, blunt tip
9.3	65	3.5	7.7	n-Si	1	Concave profile, smooth surface, blunt tip
9.3	65	4.0	7.7	n-Si	1	Slightly concave profile, smooth surface, blunt tip
7	65	4.0	7.7	n-Si	1	Smooth surface, rough profile, tip relatively sharp
4.7	65	5.0	7.7	n-Si	1	Profile slightly convex, tip sharp, "orange peel" surface
3.5	65	5.0	7.7	n-Si	1	Blunt tip, profile convex, "orange peel" surface
4.7	50	4.0	7.7	n-Si	1	Sharp tip, profile rather rough, "orange peel" surface
4.7	50	4.0	20	n-Si	1	Sharp tip, smooth profile, surface very smooth

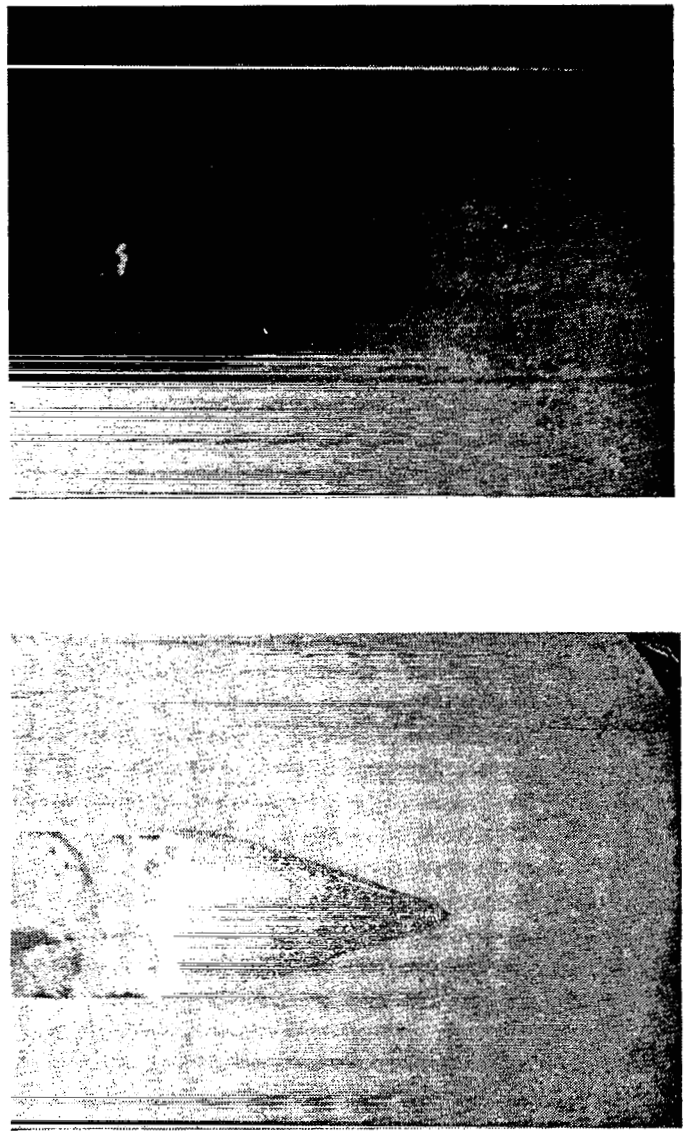

Fig. 2-7. Photomicrograph of Two Silicon Needles Fabricated Using Optimum Parameters of Table I (1 Ω-cm n-type silicon).

The stress sensitivity of p-n junctions depends, among other factors, on the ratio of stressed to unstressed junction area. Therefore, it is desirable that as much of the junction area as possible be exposed to the applied stress. The insensitivity to stress noted in some of the early needle sensors was attributed to the fact that the junction area on the tip of the needles was large with respect to that portion of this area which was actually stressed. An effort was undertaken to develop a technique of junction definition which would reduce the total junction area to that actually stressed.

The present study has been confined to the planar process for fabricating junctions on the tip of the needles. Planar needle sensors were originally fabricated by first growing an oxide on the entire silicon needle. The oxide covered needle was then coated with photoresist (such as KTFR) which remains intact after the exposure and developing process. To expose the tip of the needle, it was carefully lowered into molten black wax which defined the junction area and was then exposed to ultraviolet light. Since the area of the junction was determined by the depth to which the needle tip was lowered into the protective wax, this was the most critical and most difficult step to control in the process. It was most difficult to confine the wax to the very tip of the needle and even more difficult to mask two needles identically. Although this masking technique was somewhat successful, the need for a more precise method led to the development of other techniques.

The first technique investigated in an attempt to obtain a junction only on the portion of the needle to be stressed consisted of lowering the photoresist coated needle into a glass beaker until the needle tip

came into contact with the bottom of the beaker. The beaker was then filled with black ink for the purpose of attenuating the exposure light. The idea here was that only the very tip of the needle would touch the glass and that only this portion of the photoresist would be exposed when light was passed through the bottom of the beaker. This method did not prove to be successful and was, therefore, abandoned.

The next attempt consisted of lowering the photoresist coated needle onto a spring loaded metal plate in much the same manner as if stress was being applied to a finished sensor. The metal plate was coated with black paint so as to protect the portion of the needle in contact with the metal from the exposure light. Once contact was made, the unprotected photoresist on the needle was exposed with an ultraviolet light source for a period of approximately 2 minutes.

The needle sensors produced by the latter method were very sensitive to stress and diodes formed by using this process possessed very good electrical characteristics. Good needle sensors have been obtained by this procedure using both n and p-type silicon starting material of various resistivities. Some of the advantages of this technique over the black wax method are (1) smaller junction area definition and (2) more controllable junction definition. This technique is also much easier and faster than any other method tried to date.

Following the exposure operation, the photoresist was developed leaving a hole in the photoresist on the apex of the needle. The needles were then placed in HF to etch a hole in the oxide on the unprotected needle tip. Care must be exercised in the etching operation to insure that the photoresist does not peel off. This is best accomplished by using a pilot wafer on which the etch time is determined.

A p-n junction can be formed on the apex of the needle by simply removing the photoresist and placing the needle into an appropriate diffusion furnace. Single junctions with excellent electrical characteristics have been formed using the above process.

Junction depth and impurity surface concentration are important in the stress response of diode sensors. A shallow junction ($\sim$ 1/2 micron) with a high surface concentration ($\sim 10^{21}$ atoms/cm^3) has proved to result in the best sensors. High surface concentration not only increase the stress sensitivity of the sensors but it also makes it easier to obtain good ohmic contact to the needle tip with ordinary metals such as Au and Al.

The stress sensitivity of single junction needle sensors depends heavily on the radius of curvature of the needle point and on the junction area. Since the radius of curvature of the needle points are controllable above a few microns, it is possible to choose almost any desired sensitivity. Typical sensors fabricated in the laboratory have used a radius of curvature of approximately 1/2 mil which resulted in sensors requiring a force of approximately 10 grams to bias the device. The electrical characteristics of a typical sensor is shown in Fig. 2.8 for several stress levels.

The feasibility of fabricating multijunctions on the apex of silicon needles has been investigated. The particular device chosen for this study was a four-layer (three junction) diode. The break-over voltage of four-layer switches is stress dependent which makes the device particularly attractive for use in an oscillator configuration. The method studied for the fabrication of four-layer switch needles was identical to that used in fabricating single

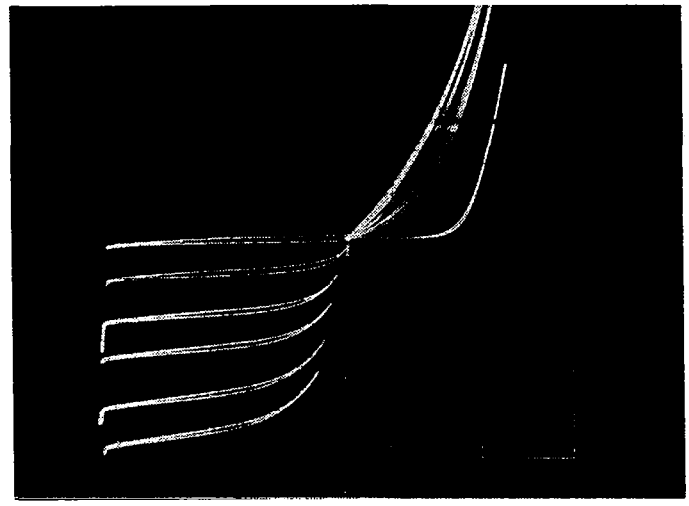

Fig. 2-8. Needle Diode Current-Voltage Characteristics for Several Stress Levels. Vertical Scale - 0.01 ma/div, Horizontal 0.2 V/div for Forward Bias and 5 V/div for Reverse Bias.

junction devices as described above except three consecutive diffusions were performed instead of one.

The problem of fabricating four-layer switches in which all three junctions are diffused junctions is difficult when all the planar processing steps are available. That is, when a new oxide can be grown and a new hole (smaller area) cut in the oxide after each diffusion step as is common in the planar process. Epitaxial substrates are much easier to work with in making multijunction devices. Aside from the masking problem in all diffused junction four-layer diodes each consecutive diffusion must be much heavier than the previous one at the expense of controlled junction depth and the quality of the junction formed.

Since it is not practically feasible using the needle structure to cut more than one window in the oxide on the apex of the needle, it is therefore necessary to carry out all diffusion through a single oxide window.

Considerable effort was put into fabricating four-layer diodes on silicon wafers utilizing a single window for the diffusion. The final process consisted of first making a very shallow (less than 1/2 micron) diffusion with a low surface concentration. This was followed by a drive-in cycle in a neutral furnace, at 1300° C, for approximately six hours. This resulted in a junction depth of approximately 10 to 15 microns. This was followed by two more diffusions with opposite type impurities. The yield on these devices was very low. The problem was not so much control over the diffusions as it was shorted junctions at the oxide junction interface. Another problem was large variations in the device properties, even for devices made at the same time. An analysis of these results showed that these variations resulted in large part from surface effects.

Attempts to translate the single window planar process for four-layer diodes to the silicon needle were unsuccessful. Although a few needle four-layer diodes were formed, they had very poor electrical characteristics. The results indicated, however, that such a process is possible if perfected and controlled properly. It is felt that a near pilot line operation would be required to perform an adequate evaluation of the process. Since neither the funds nor the equipment were available under the present study, further studies were not made.

2.9 Stress and Displacement of Needles Under an Applied Force

The following analysis of silicon needles under loaded conditions is based on needles with circular symmetry, i.e., the shank is assumed to be round. Figure 2-9 shows a sketch of the geometry considered. Silicon is shown in the figure as the pressure plate (base) onto which the needle tip is pressed. Stainless steel, silicon and quartz have been used as base materials.

If the applied force is F, then the displacement of the shank, $\Delta\ell_1$, is

$$\Delta\ell_1 = \frac{F\ell_1}{\pi a^2 E} , \tag{2.1}$$

where E is Young's modulus and a is the radius of the shank. The displacement of the conical section, $\Delta\ell_2$ is

$$\Delta\ell_2 = \frac{F\ell_2}{\pi aRE} , \tag{2.2}$$

where R is the radius of curvature of the needle point.

To calculate the displacement of the point, it is assumed that the base dimensions are much greater than the radius of the point. The displacement of the point and the base combined, Δy, is approximately[14]

$$\Delta y \simeq 1.5\sqrt[3]{\frac{F^2}{E^2 R}} \tag{2.3}$$

The total displacement of the needle under an applied force F is then

$$\Delta\ell \simeq \frac{F\ell_1}{\pi a^2 E} + \frac{F\ell_2}{\pi aRE} + 1.5\sqrt[3]{\frac{F^2}{E^2 R}} . \tag{2.4}$$

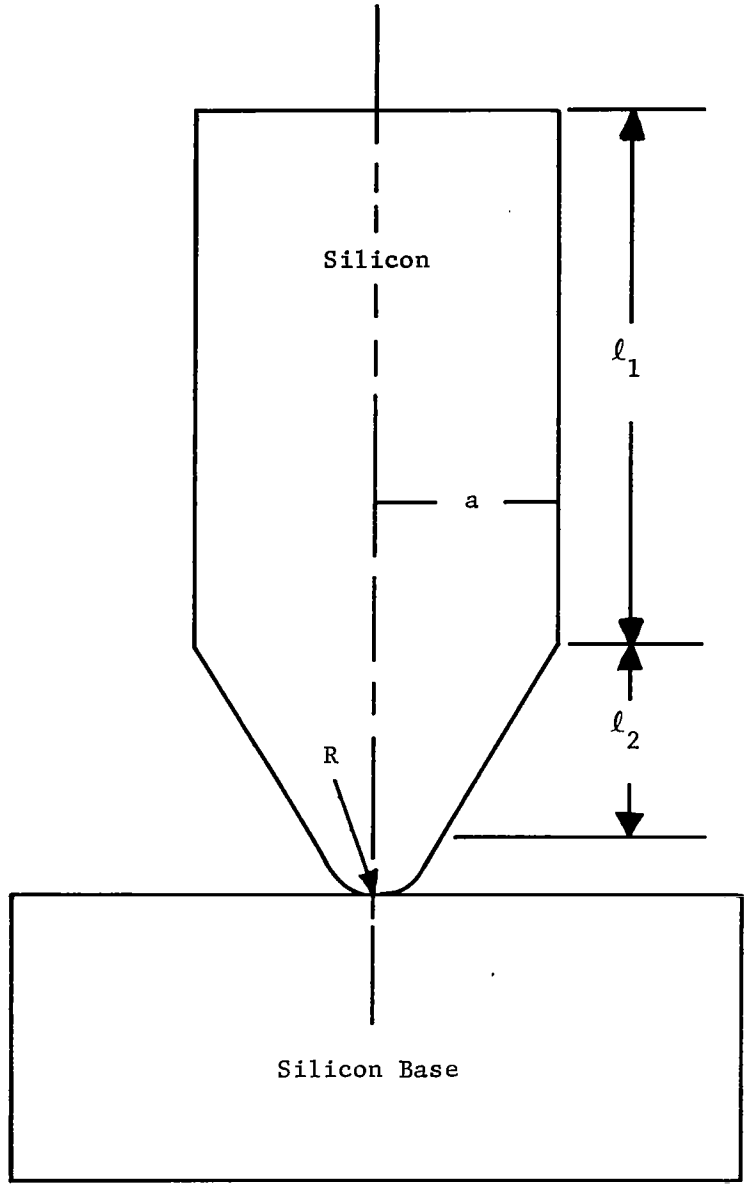

Fig. 2-9. Needle Configuration Used for Calculating Displacement.

As an example, consider a needle with the following typical dimensions:

$$R = 1 \text{ mil}$$

$$\ell_2 = 1/8 \text{ in.}$$

$$\ell_1 = 1/4 \text{ in.}$$

$$E = 1.7 \times 10^{12} \text{ dynes/cm}^2 .$$

In this case:

$$\Delta y \simeq 8 \times 10^{-6} \, F^{2/3} \text{cm}, \quad (F \text{ in grams})$$

$$\Delta \ell_1 \simeq 0.17 \times 10^{-6} \, F$$

$$\Delta \ell_2 \simeq 0.9 \times 10^{-6} \, F$$

As can be seen, the total displacement per gram load is approximately one tenth of a micron which is very small. In fact, for most applications, the displacement of the needle can be neglected in comparison to the displacement of the housing or mechanical configuration.

The relationship between stress in the needle tip and applied force is very complicated. This problem has been considered by a number of workers.[15-18] In order to calculate the effects of stress on junction properties, it is necessary to know the stress as a function of position in the needle tip. This is a formidable problem, the solution of which is not at present worth the effort required to obtain it. There has been some success with the evaluation of an indenter point in contact with a planar junction structure.[15]

Since the function $\gamma_\nu (\sigma)$, which is of particular interest here, is an exponential function of stress, the maximum stress is important. The pressure on the surface under the contact is[18]

$$\sigma = \frac{3F}{2\pi a^2}\sqrt{\frac{a^2 - r^2}{a^2}} , \tag{2.5}$$

where a is the radius of the contact circle and r is the distance from the center to the point of interest. The radius of contact, a, is[18]

$$a = \sqrt[3]{\left(\frac{1 - \nu^2}{E}\right)\ (3/2)RF} , \tag{2.6}$$

or

$$a = K(RF)^{1/3} , \tag{2.7}$$

where ν is Poisson's ratio. The maximum stress is then

$$\sigma_{max} = \frac{3F}{2\pi a^2} , \tag{2.8}$$

or

$$\sigma_{max} = K_2\ F^{1/3} . \tag{2.9}$$

At high stress levels such that $\gamma_\nu(\sigma) = C_1\ \exp(C_2\sigma)$

$$\gamma_\nu(\sigma) \simeq C_3\ \exp(C_4 F^{1/3}) . \tag{2.10}$$

For very shallow junction depths such that the stress is not very different from that at the surface, one would expect the above formulas to be reasonably accurate.

The average stress on the needle tip is

$$\sigma_{ave} = \frac{F}{\pi a^2} . \tag{2.11}$$

Note that the average differs by a factor of 2/3 from the maximum. The effective value needed in making computations is somewhere between the average and the maximum.

2.10 Electrical Response of Silicon Needle Diodes Under Stress

The single junction silicon needle has been the most used sensor in this study. The following discussion considers, theoretically, the electrical response of such devices under stress. The forward and reverse biased current-voltage characteristics of diodes under stress are considered in I. Both the "ideal" and generation-recombination currents are considered. The total current as a function of voltage and stress (stress is represented by $\gamma_v(\sigma)$) for a uniformly stressed junction is given in Eqs. 1.3 and 1.4.

Generally speaking, the most promising mode of operation for a diode needle sensor is the constant voltage mode in which the diode current is used as the stress indicator. The current is exponentially related to stress through $\gamma_v(\sigma)$ while the voltage is linearly related to stress. The current is, therefore, more sensitive than voltage. For the present purposes, it is assumed that voltage is held constant. Also, since the sensors used were with a dc bias force, the approximation

$$\gamma_v(\sigma) = C_1 e^{C_2\sigma}$$

is a good assumption. The current can be written as follows

$$I_T = K_1 e^{C_2\sigma} + K_2 e^{C_2\sigma/2}, \qquad (2.12)$$

where K_1 and K_2 are constants that depend on the magnitude and polarity of the voltage, unstressed current, crystal orientation and temperature.

Normally, K_1 will be much larger than K_2 in the forward biased condition while K_2 will be much larger than K_1 in the reverse biased state. Since both terms in Eq. (2.12) have the same functional relationship on σ, only one term will be considered further, i.e.,

$$I = K_3 \, e^{C_1 \sigma} \quad . \tag{2.13}$$

As can be seen from Eqs. (2.9) and (2.11), σ is expected to be proportional to $F^{1/3}$. If the total junction area is stressed, then the diode current is functionally related to force as follows:

$$I = K_3 \, e^{CF^{1/3}} \quad . \tag{2.14}$$

In most practical sensors, it is more likely that only a part of the junction is stressed. In this case, if A is the total junction area and A_S is the stressed area, the current is

$$I = \frac{A - A_S}{A} K_4 + \frac{A_S}{A_T} K_5 \, e^{CF^{1/3}} \quad . \tag{2.15}$$

The stressed area is related to the radius of contact by

$$A_S = \pi a^2 \quad . \tag{2.16}$$

The contact radius is proportional to $F^{1/3}$ as shown in Eq. (2.7). Therefore, $A_S \propto F^{2/3}$. The current is then related functionally to the applied force as follows:

$$I = K_4 - K_6 F^{2/3} + K_7 F^{2/3} \, e^{CF^{1/3}} \quad . \tag{2.17}$$

If $A >> A_S$, Eq. (2.17) reduces to

$$I = K_1 + K_7 F^{2/3} e^{CF^{1/3}} \tag{2.18}$$

In utilizing the needle sensor in practical transducers, it will be necessary to calibrate the current-voltage characteristics as a function of applied force. Although the functional relationships aid in the design of devices and an understanding of their behavior, the approximations made in the theory are not good enough and the models on which they are based are not accurate enough for device use. This does not mean, however, that the needle sensor is not good. Like almost all of the conventional transducer sensors that are commercially available, they must be calibrated individually.

Section III

ACCELEROMETER DEVELOPMENT

3.1 Introduction and Discussion

One of the major goals of this study has been to design, fabricate, and demonstrate a laboratory accelerometer based on the piezojunction effect. Emphasis has been placed on the silicon needle sensor as the transducing element in the accelerometers. Although a variety of configurations have been studied, they have all been of the diaphragm or beam type. The configuration found to be the best is the double-diaphragm type.

The general case of an accelerometer based on the silicon needle sensor is shown schematically in Fig. 3-1. A dc force biasing spring

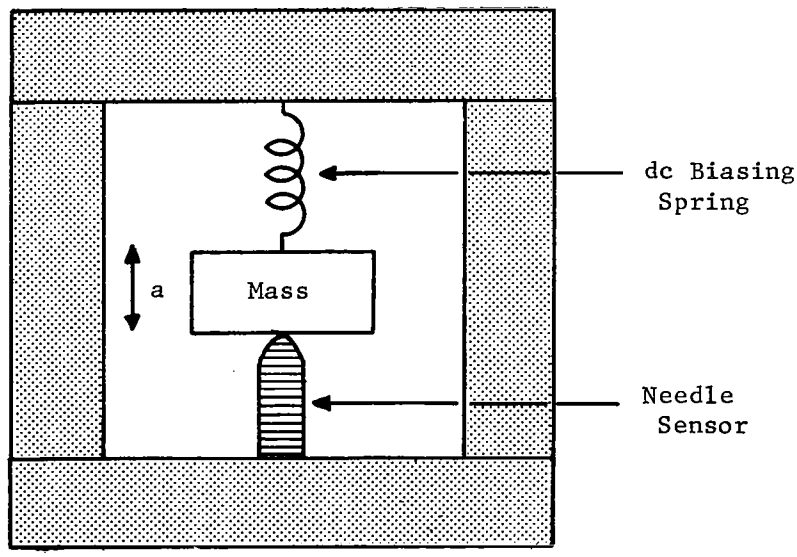

Fig. 3-1. Schematic of a General Accelerometer Utilizing the Needle Sensor.

is shown in the figure. This spring can be anything from an actual spring to the give of the mechanical housing holding the mass in place under the bias force applied to the needle.

As discussed in Section 2.4, the displacement of the needle under an applied force F is

$$\Delta\ell \simeq \frac{F\ell_1}{\pi a^2 E} + \frac{F\ell_2}{\pi a R E} + 1.5\sqrt[3]{\frac{F^2}{E^2 R}} \tag{2.4}$$

This displacement of the needle is important in the dynamic operation of an accelerometer which utilizes the needle sensor. Although $\Delta\ell$ is not linearly related to F, it is approximately linear for small changes in F. It will be assumed for the present purposes that

$$F \simeq K_e \ell \tag{3.1}$$

where K_e is the equivalent spring constant of the needle which can be calculated from Eq. (2.4).

The dynamic configuration for the accelerometer of Fig. 3-1 is shown in Fig. 3-2. As shown in the figure, K_s is the effective spring constant of the biasing spring and the mechanical housing and M_s is the effective mass of the spring. The resonant frequencies of the system are

$$f = \frac{1}{2\pi}\left\{\frac{1}{2}\left[\left(\frac{K_e}{M} + \frac{2K_s}{M} + \frac{4K_s}{M_s}\right) \pm \left(\frac{K_e^2}{M^2} + \frac{4K_s K_e}{M^2} - \frac{8K_s K_e}{MM_s} + \frac{4K_s^2}{M^2} + \frac{16K^2}{M_s^2}\right)^{\frac{1}{2}}\right]\right\}^{\frac{1}{2}}. \tag{3.2}$$

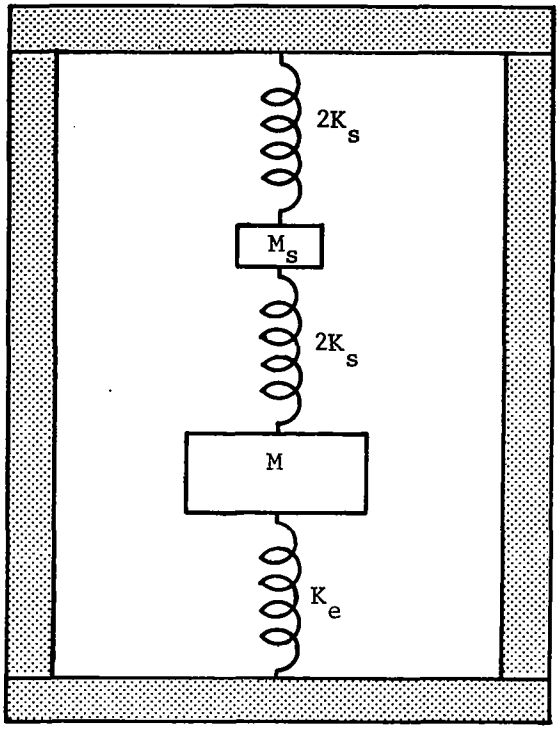

Fig. 3-2. Mechanical Equivalent of an Accelerometer.

If $M_s \ll M$, the fundamental frequency of Eq. (3.2) reduces to

$$f = \frac{1}{2\pi}\sqrt{\frac{K_s + K_e}{M}} \quad . \tag{3.3}$$

The assumption that $M_s \ll M$ is good for low and medium g accelerometers. Also, K_s will normally be much less than K_e.

Using the example of Section 2.4 for the needle sensor and a two gram seismic mass the lowest possible resonant frequency ($K_s = 0$) is approximately 3.7×10^3 cps. An accelerometer utilizing this needle

and the two gram weight would, therefore, have a minimum resonant frequency of 3.7 kc.

In the static case where there is no mechanical advantage or disadvantage obtained from the device, the force on the needle is simply,

$$F = Mg + F_o \tag{3.4}$$

where g is the acceleration level and F_o is the dc bias force.

3.2 Single-Diaphragm Accelerometers

The single-diaphragm accelerometer consists of a cylindrical seismic mass supported by a circular diaphragm with a needle sensor in contact with the diaphragm on the side directly opposite the mass. The diaphragm is clamped or fixed at the edges. Figure 3-3 is a sketch of the accelerometer.

The deflection of the center of the diaphragm is

$$\Delta y = \frac{3(Mg - F)(m^2 - 1)}{4\pi m^2 E t^3}\left[a^2 - b^2 - \left(\frac{4a^2b^2}{a^2 - b^2}\right)\left(\log \frac{a}{b}\right)^2\right], \tag{3.5}$$

where Δy = displacement of the mass

M = seismic mass

m = reciprocal of Poisson's ratio

E = Young's modulus of diaphragm

t = diaphragm thickness

g = acceleration in g's.

Equation (3.5) can be used to calculate the spring constant of the diaphragm.

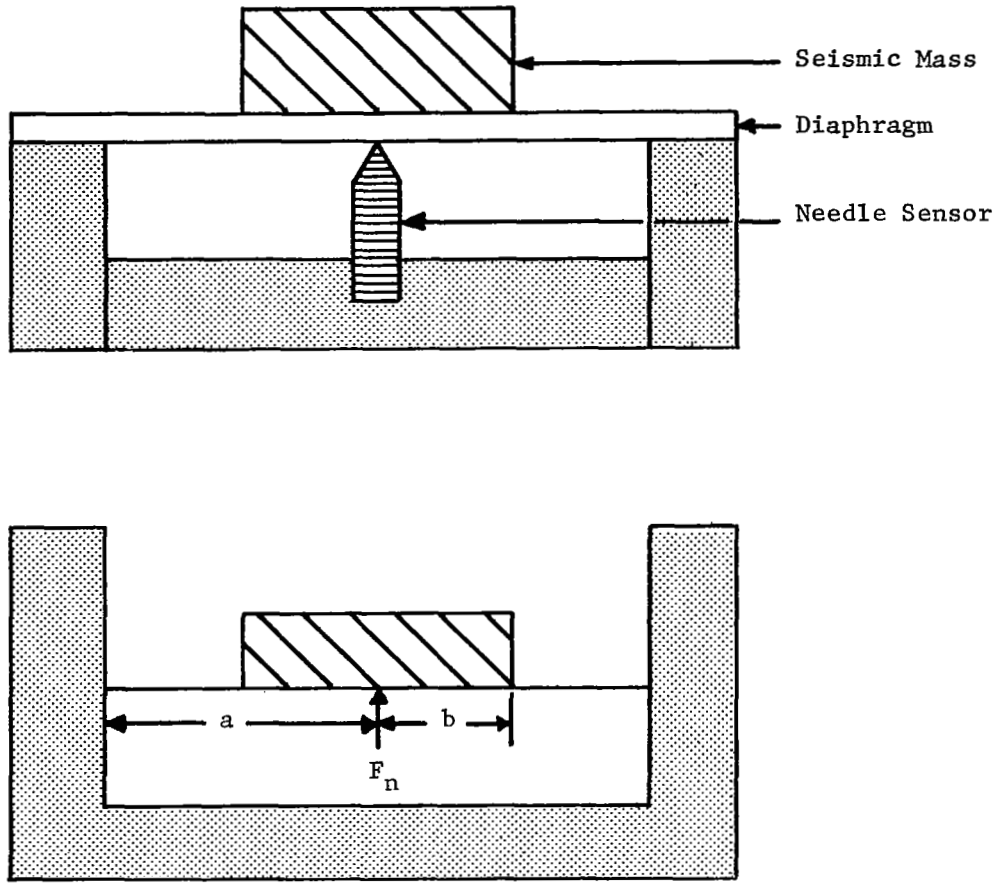

Fig. 3-3. Sketch of Single-Diaphragm Accelerometer.

The dc bias force can be applied in the diaphragm accelerometer by simply constructing the device so that the needle is exerting the desired force against the diaphragm. The diaphragm acts in this case as the biasing spring. Figure 3-4 is a photograph of a single-diaphragm accelerometer in which the diaphragm is used as the biasing spring. The device consists of a brass base in the center of which a silicon needle sensor is soldered, a glass housing, a brass diaphragm (2 mils thick), and the seismic mass. The device is fabricated by first

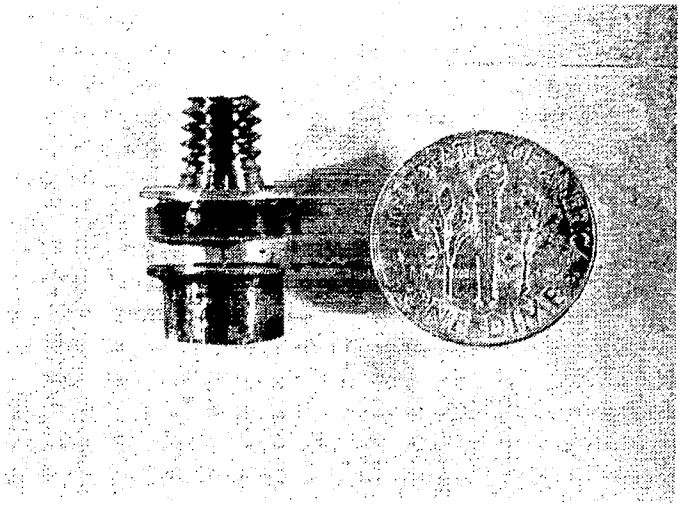

Fig. 3-4. Photograph of a Single-Diaphragm Accelerometer.

soldering the mass to the diaphragm. The diaphragm is then epoxied to the glass housing. The next step is to attach the needle sensor to the base. This is done by drilling a hole the size of the needle and soldering the needle shank into the base. The final step consists of epoxying the base to the housing. During the curing cycle for the final step, a constant force is maintained between the glass housing and the base to create the desired dc bias force. Electrical contact is made between the diaphragm and the base.

The needle diode sensors used in accelerometers of this type were pressed into the brass diaphragm. Subsequent tests of these accelerometers showed large hysteresis and drift effects which were eventually

traced to the plastic deformation of the brass under the needle point. Each time the devices were accelerated to a new high acceleration level the devices exhibited a new set of electrical characteristics as a function of acceleration. Since there were no means provided for the adjustment of the dc bias force, the devices usually failed by losing electrical contact to the needle sensor.

In addition to the above mentioned problems, the single-diaphragm accelerometers were found to be sensitive to cross-axes acceleration. This was not an unexpected result since a cross-axes acceleration applies a large moment on the diaphragm due to the mass and height of the seismic mass.

Some improvements were incorporated into the single-diaphragm accelerometers. One of the improvements was to use stainless steel as the diaphragm material. Another improvement was the use of an adjustable bias force. The latter was accomplished by mounting the needle on the end of a screw which was then threaded into the base. Since the needle rotates with respect to the diaphragm during the assembly operation, it was necessary to pull up on the diaphragm until the needle was inserted to the desired height and then release the diaphragm to allow it to make contact with the needle. This prevented breakage of the needle.

Although the single-diaphragm accelerometer is relatively easy to construct, its cross-axes sensitivity, especially for applications in the low g range, make it unattractive compared to other devices such as the double-diaphragm type.

3.3 Double-Diaphragm Accelerometers

The double-diaphragm accelerometer was designed to eliminate the cross-axes sensitivity problems associated with the single-diaphragm type. A schematic drawing of the double-diaphragm type is shown in Fig. 3-5. The second diaphragm prevents the mass from rotating under cross-axes acceleration.

For the case where both diaphragms are identical, the displacement of the mass is given by Eq. (3.5) with (Mg - F) replaced by (Mg - F)/2.

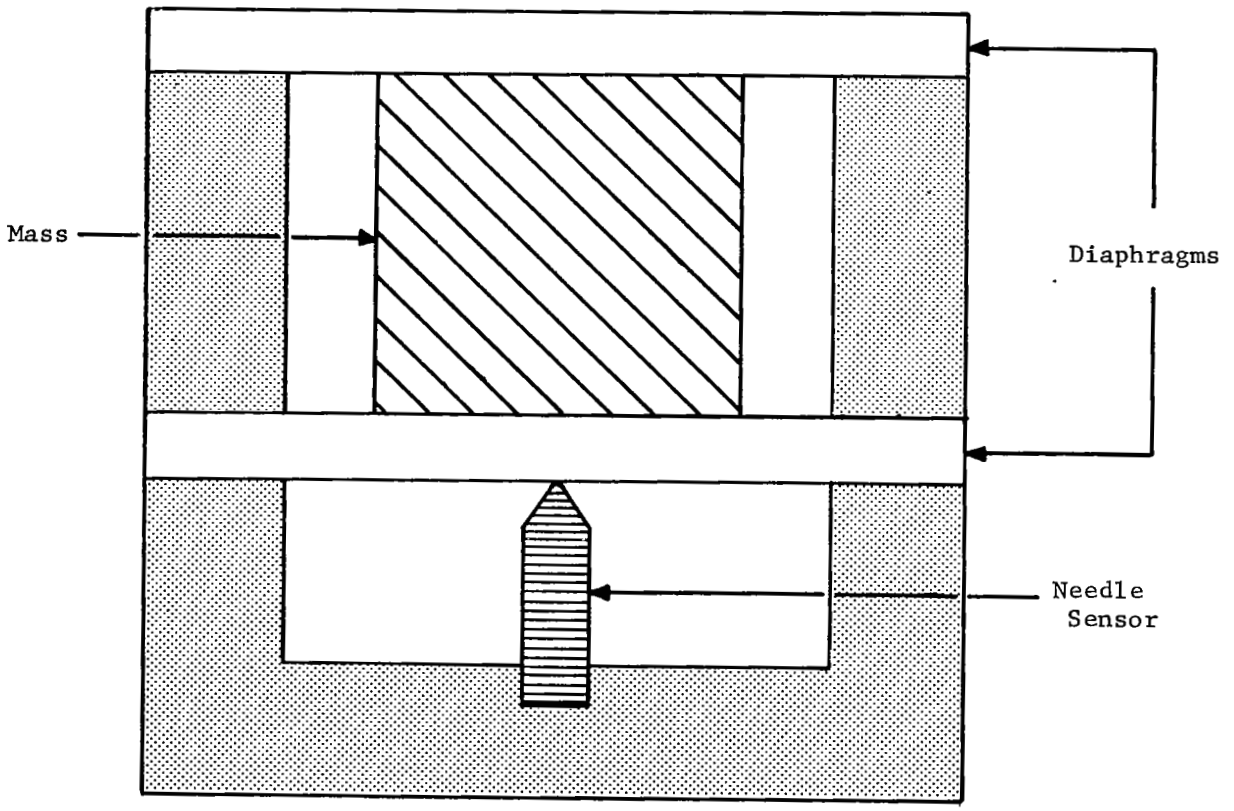

Fig. 3-5. Schematic of Double-Diaphragm Accelerometer.

In cases where the two diaphragms are different, Eq. (3.5) must be applied for each diaphragm with (Mg - F) replaced by (Mg - F - Q) for one and Q for the other. The two equations are then solved simultaneously.

A variety of double-diaphragm accelerometers have been fabricated and tested. Based on the results obtained on the single-diaphragm type and other types, it was decided in the beginning that an adjustable dc bias force was necessary. Since there is always some relaxation of the mechanical housing and some plastic deformation of the needle and its base, the adjustable bias was incorporated into the design. Figure 3-6 shows a schematic representation of the accelerometer showing the

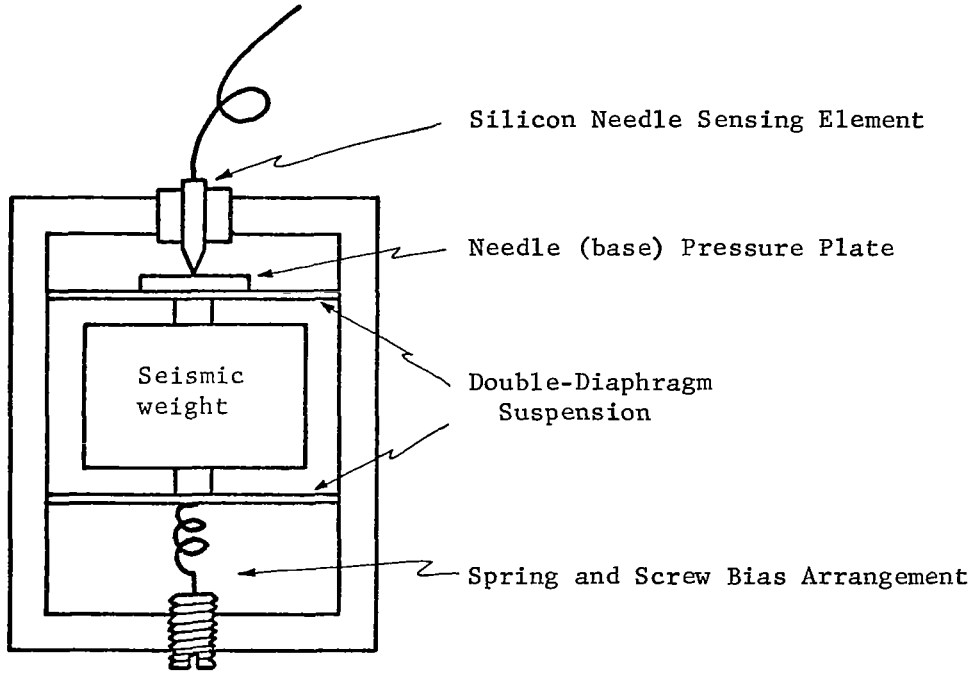

Fig. 3-6. Schematic Representation of a Double-Diaphragm Accelerometer Showing the dc Bias Adjustment Arrangement.

dc bias adjustment arrangement. For this type of arrangement, the equivalent spring constant of the diaphragms and the spring is obtained by simply adding the spring constant of the bias spring, K_b, to the spring constant of the diaphragms, i.e.,

$$K_e = K_d + K_b \quad . \tag{3.6}$$

It should be noted that the needle is mounted on the opposite side of the diaphragms and mass from the bias spring. If it were mounted behind the needle and the needle allowed to move, the resonant frequency would be lowered considerably and the system would be extremely unstable.

A cross-section view of a typical double-diaphragm accelerometer is shown in Fig. 3-7. The housings for these devices have been brass, with 10-32 screw threads on the bottom for mounting purposes. The housing is electrical ground and the other electrical lead is attached to the needle shank. The shank of the needle sensor is electrically isolated from the accelerometer housing.

The diaphragms are soldered to the center housing ring and the housing is put together with screws. The needle holder is epoxied to the top housing piece. The needle is mounted in a brass rod (holder) by soldering and the rod is then epoxied in the housing. Electrical insulation is provided by the epoxy. In the device shown in Fig. 3-7, the mass is attached to the diaphragms by screws. This can also be accomplished by epoxy or solder.

Laboratory accelerometers were tested both statically and dynamically in the Standards Laboratory at Langley Research Center,

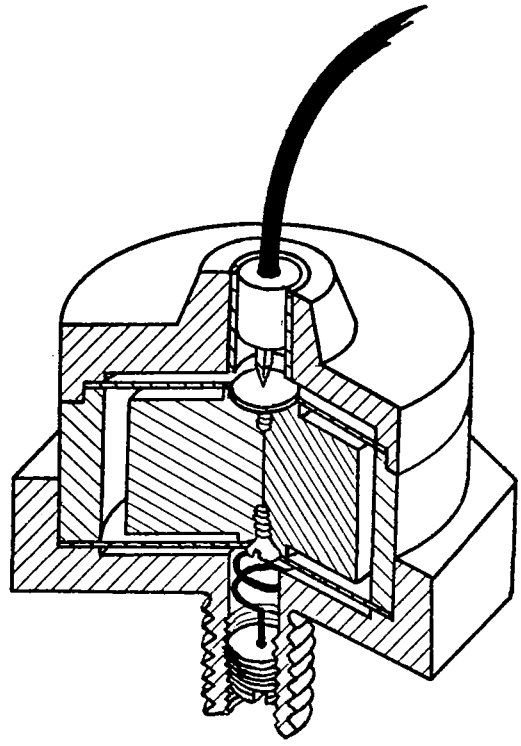

Fig. 3-7. Cross-Section of a Typical Double-Diaphragm Accelerometer.

Hampton, Virginia. In these tests, a positive acceleration was such that the seismic mass pressed against the needle sensor and a negative acceleration relieved stress on the needle.

Three series of accelerometers of the double-diaphragm type have been fabricated and tested. All three series were of the same general configuration as that shown in Fig. 3-7. The first series utilized a gold plated stainless steel pressure plate (base) for the silicon needle. The needle sensors in this set did not have any metal contact material on the tip of the needle, i.e., electrical contact was made by the silicon needle tip in contact with the gold plated steel.

Figure 3-8 is a photograph of one of the accelerometers of the first series. These devices had a 2 gram mass. The top of the accelerometer was designed to accommodate a Microdot connector for electrical contact. These devices were tested by using the current at a constant voltage as a measure of the acceleration. Figure 3-9 is a plot of ΔI as a function of acceleration with a reverse bias voltage of -15 volts. The curve is a copy of the data as recorded on an x-y plotter. As can be seen in Fig. 3-9, there is a hysteresis in the characteristics. The current did not return to its original value following an acceleration to a new high level. When tested at acceleration levels below some previous level, the loop was found to close at zero g. Another example of the hysteresis effect in another device is shown in Fig. 3-10. The top curve is the first run and the bottom curve is the second run.

Tests of cross-axes sensitivity showed that the devices had a cross-axes sensitivity of less than 1% of that in their sensitive axis. Figure 3-11 is a plot of sensitivity at a constant g level as a function of frequency. As shown, the resonant frequency was approximately 3 KC. This is slightly lower than calculated earlier. This was expected since the pressure plate was stainless steel and not silicon as had been assumed in the calculations.

Aside from the hysteresis effects in the first set of devices, the sensitivity was much lower than expected. A careful analysis of the test results showed that the low sensitivity and much of the hysteresis effects resulted from plastic deformation of the stainless steel pressure plate.

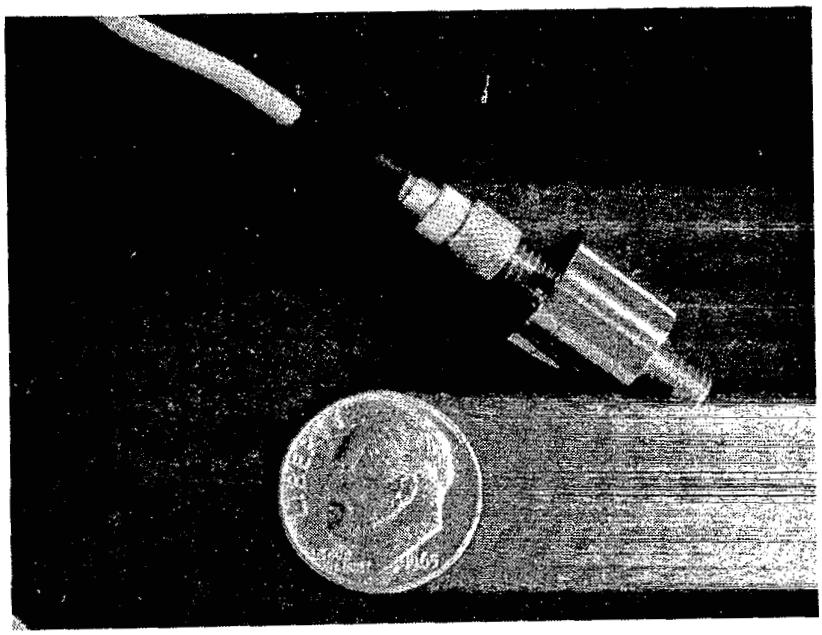

Fig. 3-8. Photograph of a Double-Diaphragm Accelerometer with a 2 gram mass.

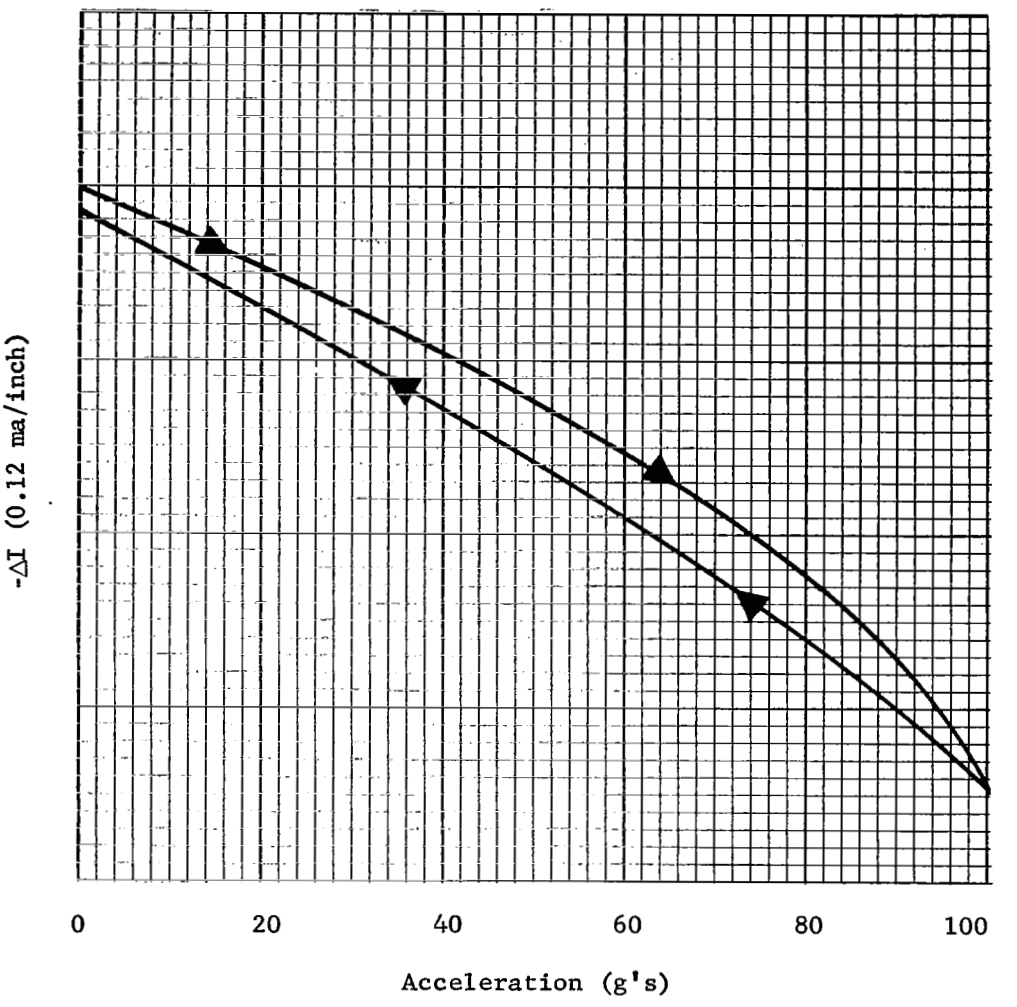

Fig. 3-9. Change in Current (V = -15 volts) as a Function of Acceleration for the Accelerometer Shown in Fig. 3-8.

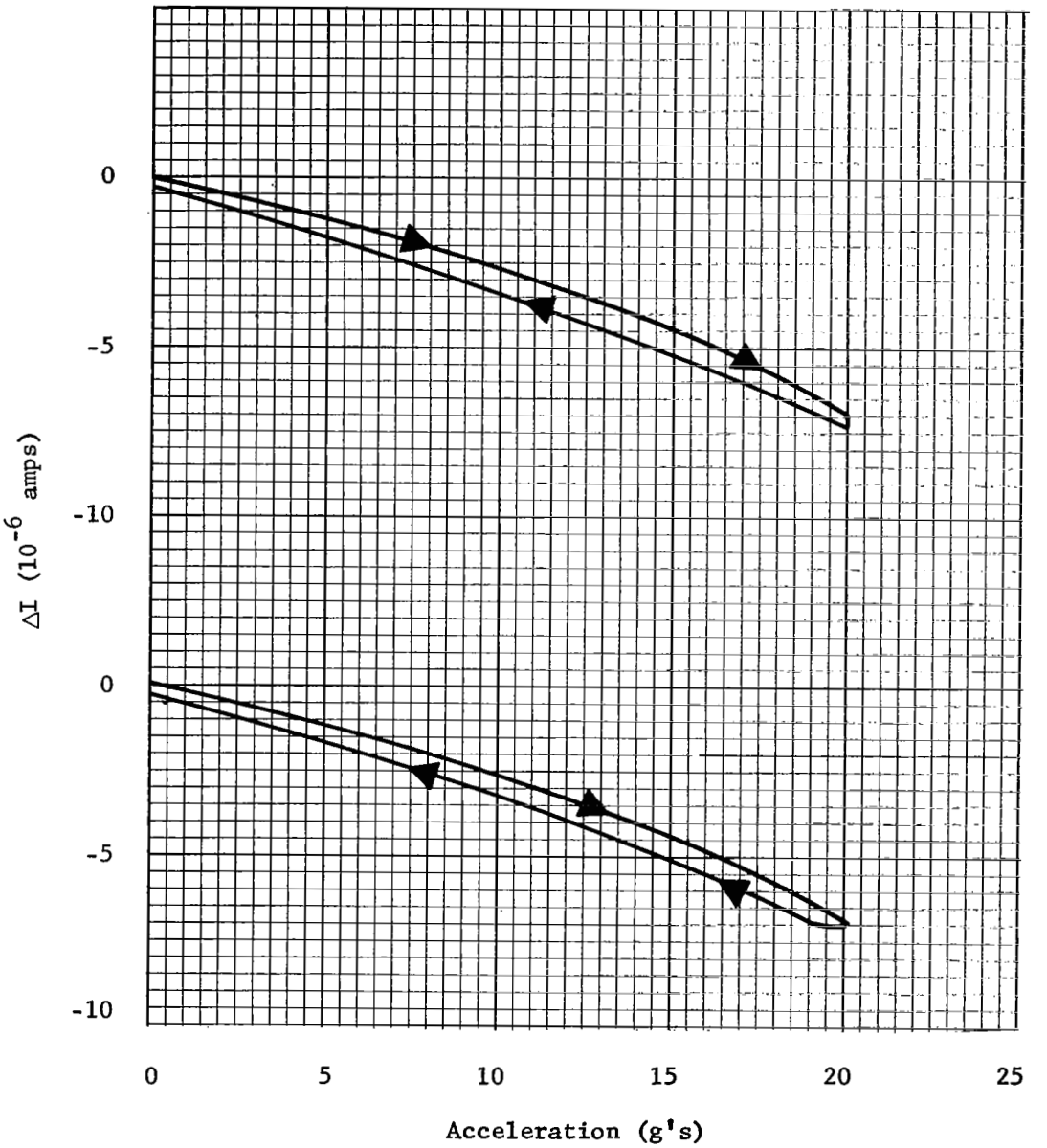

Fig. 3-10. Change in Current as a Function of Acceleration for an Accelerometer of the First Series.

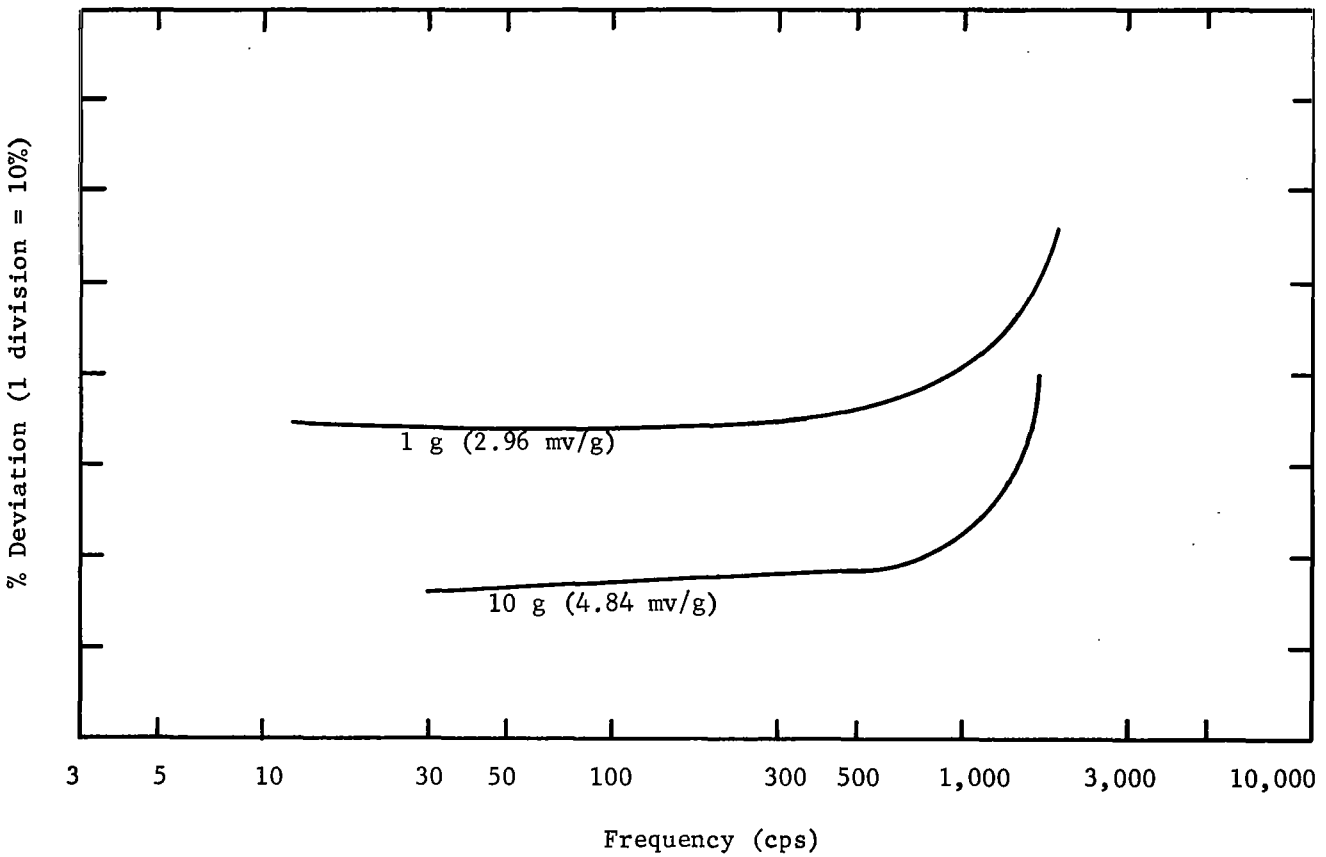

Fig. 3-11. Plot of Sensitivity as a Function of Frequency for 1 g and 10 g Sinusoidal Accelerations.

The second set of devices that were fabricated and tested were identical with the first set except the pressure plate was made of gold plated silicon. This made the mechanical properties of the pressure plate and the sensor identical. Again, these devices did not utilize any metal on the tip of the silicon needle. Although several of these devices were fabricated, all but one was broken while being transported to LRC for testing. The one remaining device was tested with the aid of the circuit shown in Fig. 3-12. The offset or bias voltage V_o is the voltage required in series with the recorder to give a zero voltage under zero g acceleration. V is the battery voltage. ΔV is the change in voltage across the 10 K resistor due to acceleration.

Figure 3-13 is the actual recorder plot of ΔV as a function of acceleration for several reverse biased conditions. As shown, the acceleration was from -5 to +5 g's. The vertical scale for ΔV is 1 volt per major division (1 inch). As shown in Fig. 3-13, both the sensitivity and the hysteresis effect increases with reverse bias voltage.

The forward biased mode is shown in Fig. 3-14. Again, the sensitivity increases with bias voltage. Note in Fig. 3-14 that two curves are shown for V = 0.4 volts. The lower 0.4 volt curve was slightly offset with the recorder zero and represents four consecutive runs to show the repeatability. As can be seen by comparing Fig. 3-13 with 3-14, the hysteresis effect is virtually non-existent in the forward biased case.

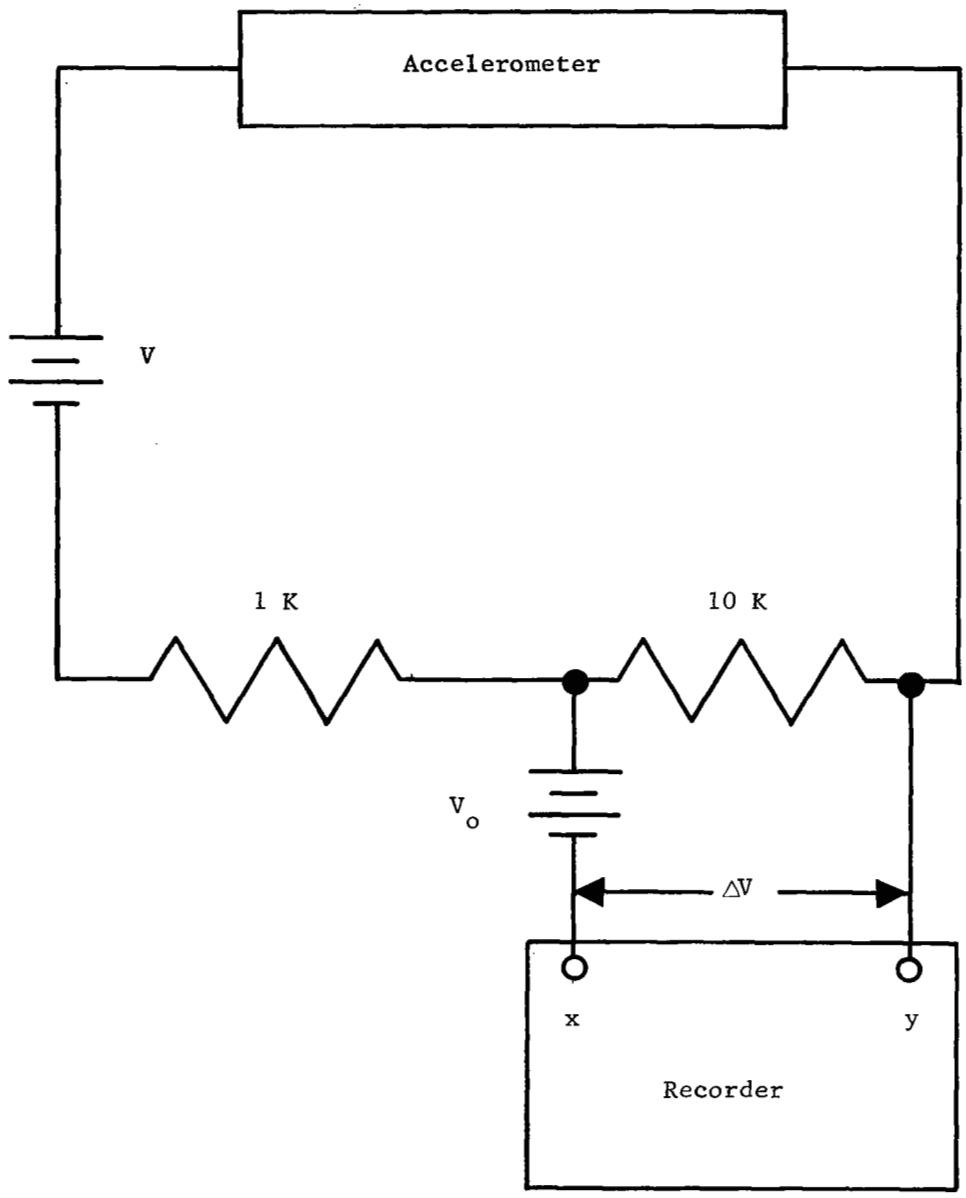

Fig. 3-12. Circuit Used to Test Accelerometers.

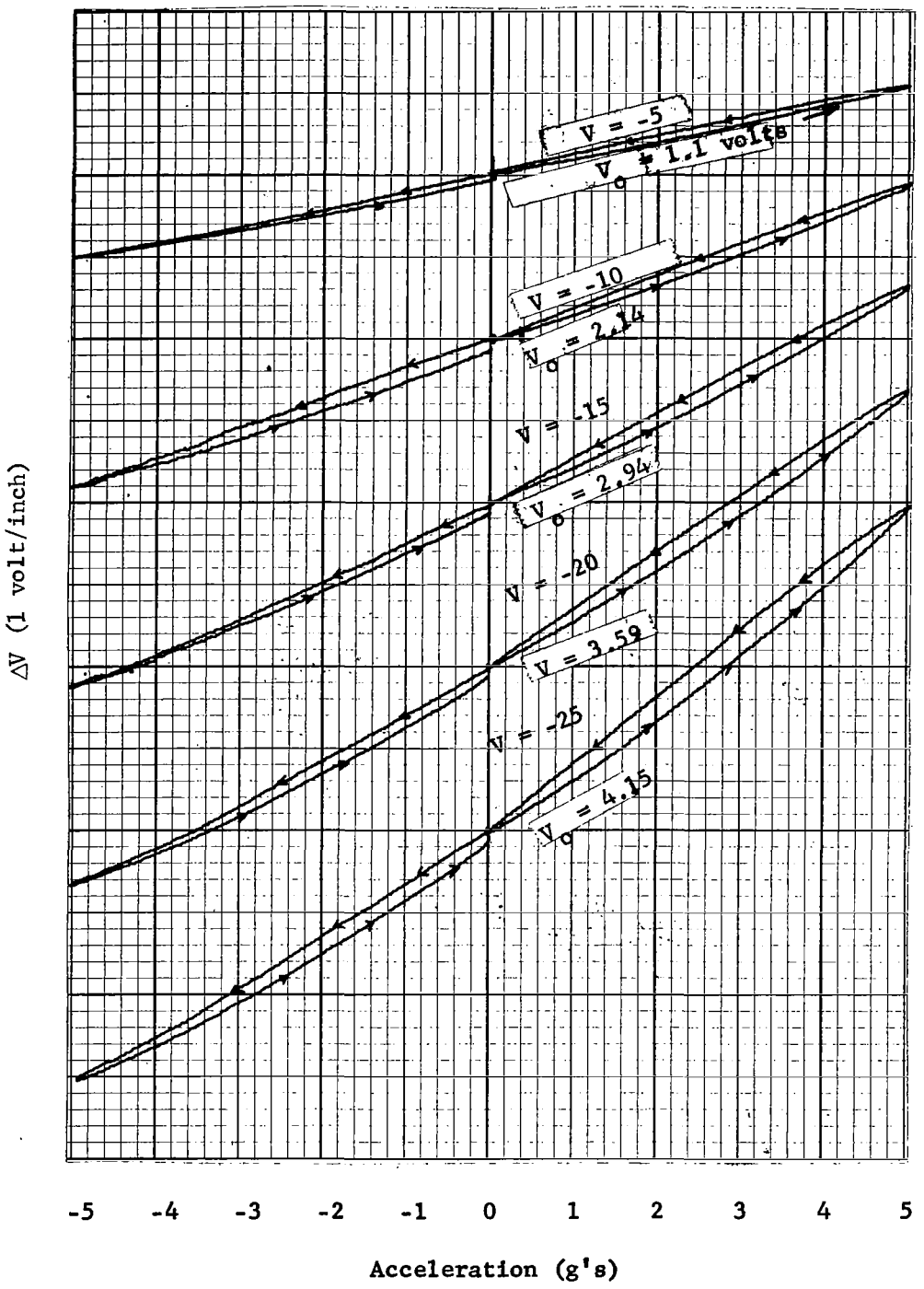

Fig. 3-13. Recorder Plot of ΔV as a Function of Acceleration for the Reverse Biased Mode. The Vertical Scale is 1 volt/major division.

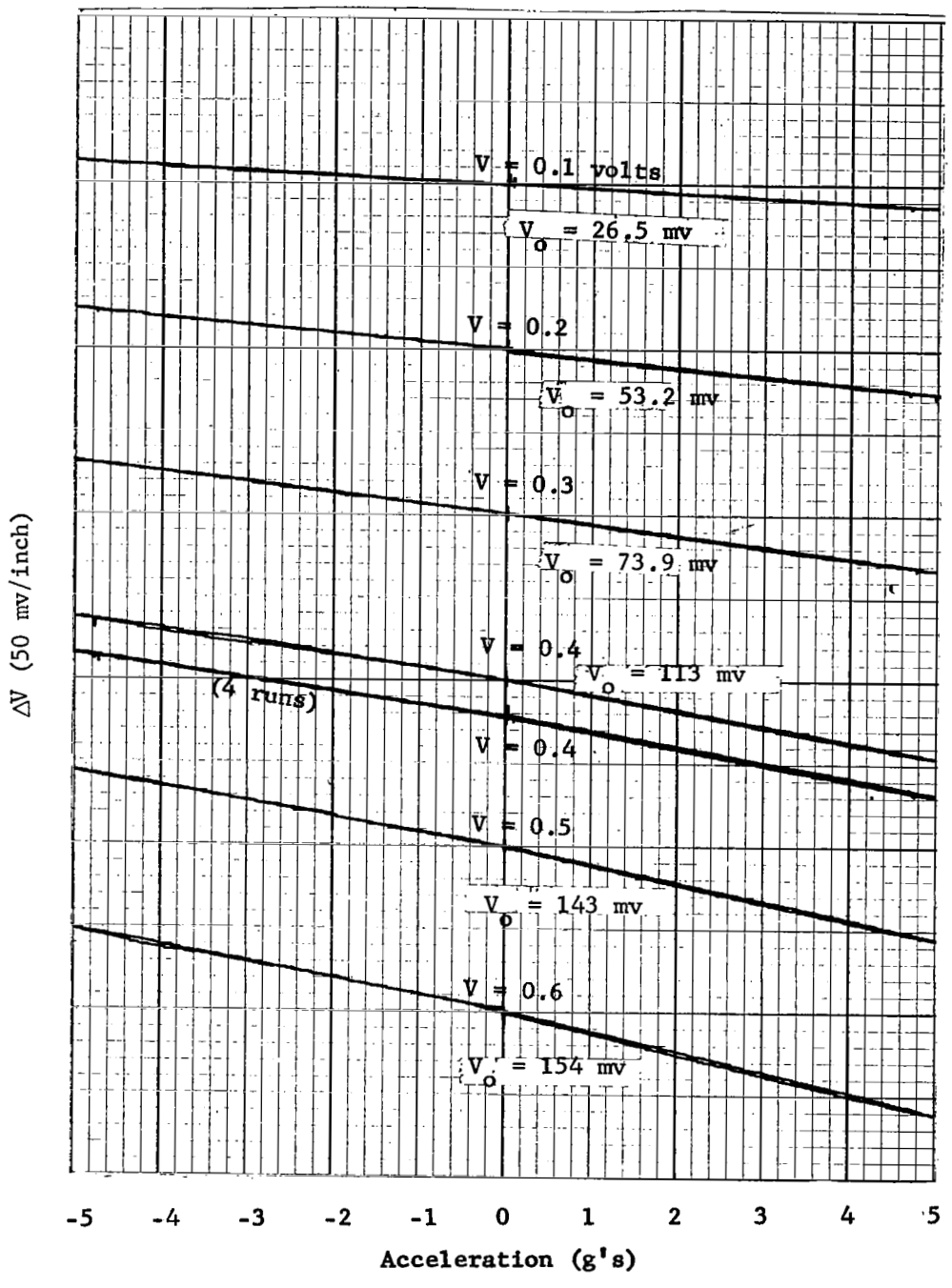

Fig. 3-14. Recorder Plot of ΔV as a Function of Acceleration. The Device was Operated in the Forward Biased Mode. The Vertical Scale is 30 mv/major division.

Figure 3-15 is a recorder plot of sensitivity for a reverse bias of -15 volts for acceleration along the sensitive axes and along the transverse axes.

The third set of devices utilized the gold plated silicon pressure plate. In addition, the needle tip was coated with an uncured insulating epoxy prior to installation of the needle into the housing. The needle point punched through the epoxy when the bias force was applied. The idea here was to add mechanical support to the needle especially for transverse motions. Also, the epoxy should provide some heat sink effects. As one might expect, the devices were plagued with poor electrical contacts. These poor contacts were experienced even though gold was plated on the needle tips prior to the epoxy.

Figure 3-16 is a photograph of one of the accelerometers of the above type. This particular device was designed to respond to low g accelerations by making the radius of curvature of the needle tip smaller than the previous devices. Figure 3-17 is a photograph of the forward and reverse current-voltage characteristics of the accelerometer under 0 and $\pm$ 1 g accelerations -- A = -1 g, B = 0 g, C = + 1 g. The vertical scale is 0.1 ma/division for both the forward and reverse modes. The horizontal side is 0.5 volts/division for the forward and -5 volts/division for the reverse mode. The non-linearity of the piezojunction effect can easily be seen in Fig. 3-17 where, for a constant voltage, the current change between 0 and -1 g is seen to be smaller than the change between 0 and + 1 g.

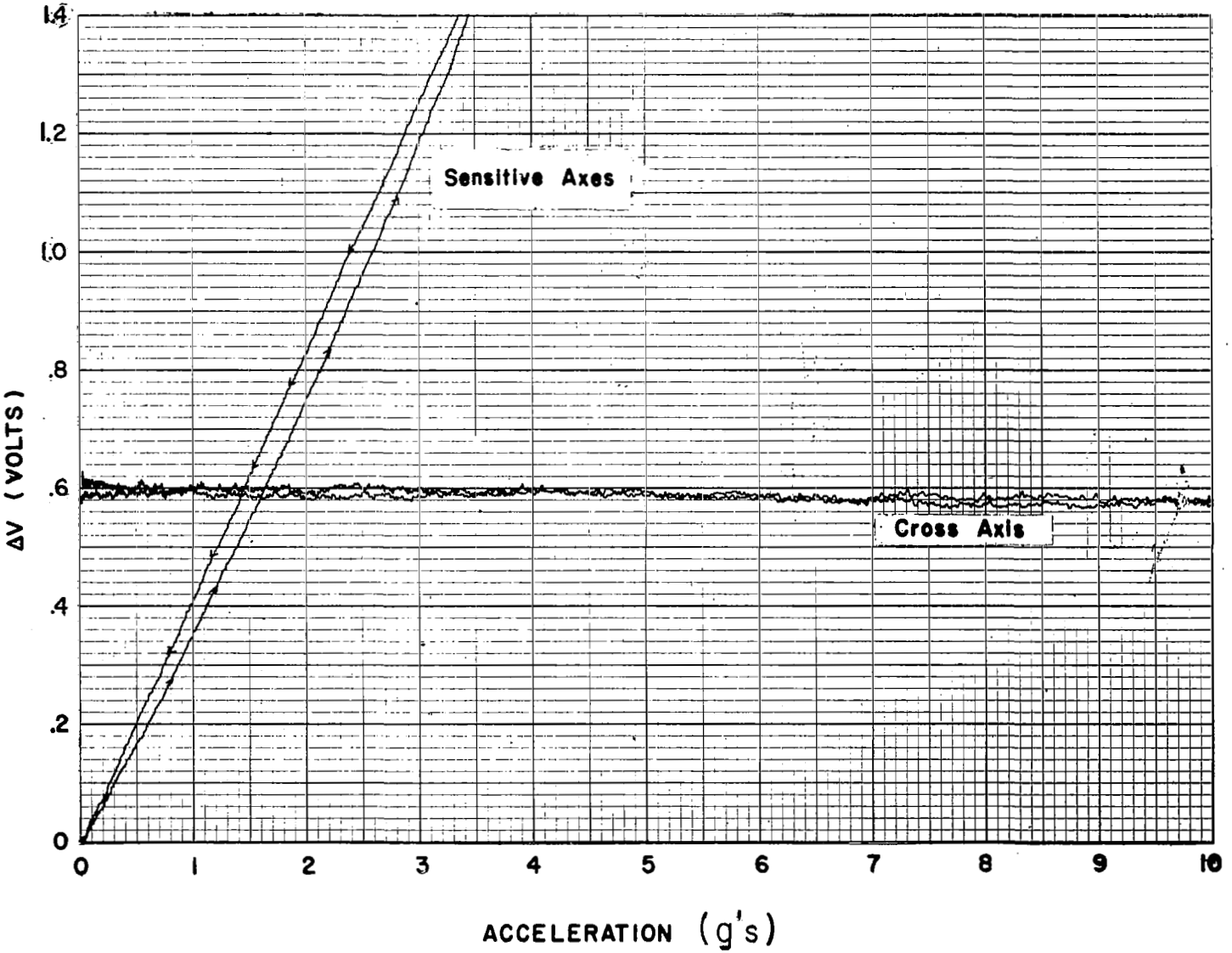

Fig. 3-15. A Recorder Plot of Sensitivity for a Reverse Bias of -15 Volts for Acceleration Along the Sensitive Axes and Along the Transverse Axes.

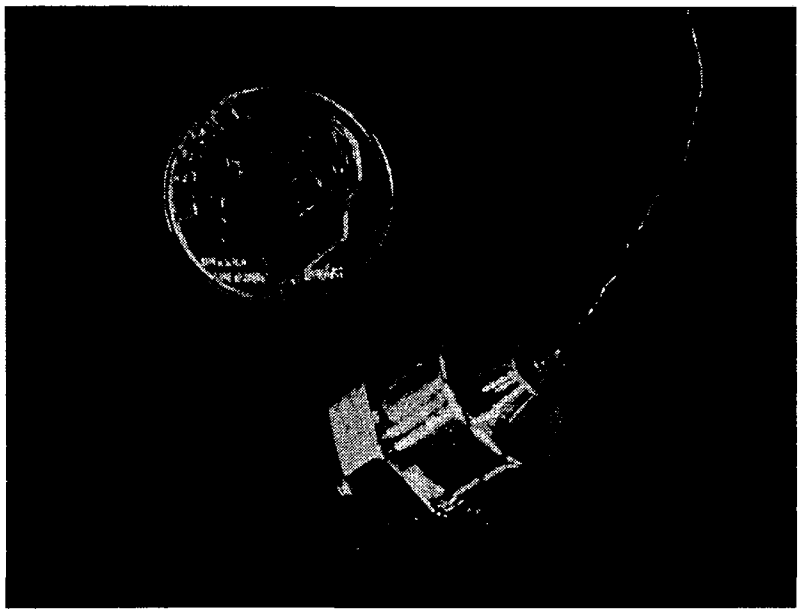

Fig. 3-16. Photograph of a Double-Diaphragm Accelerometer. No Microdot Connector is Provided.

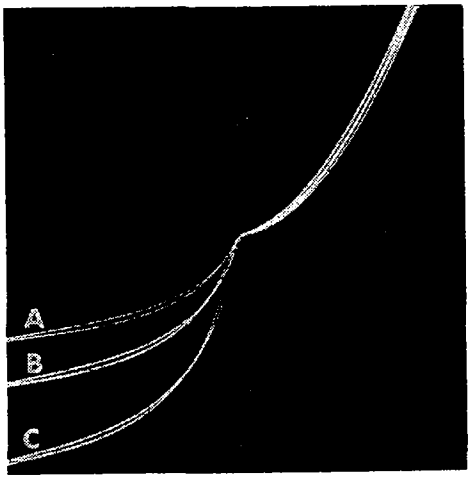

Fig. 3-17. Current-Voltage Characteristics of the ± 1 g Accelerometer Shown in Fig. 3-16. A = -1 g, B = 0 g and C = + 1 g. The Vertical Scale is 0.1 ma/div. for Both Forward and Reverse Modes. The Horizontal Scale is 0.5 V/div. for Forward and -5 V/div. for Reverse Mode.

Figure 3-18 shows a recorder plot of ΔV as a function of acceleration for several reverse biased conditions. The circuit shown in Fig. 3-12 was again used to test this device. Note that the hysteresis effects were also present with these devices and as before was found to increase with an increase in bias voltage.

Figure 3-19 shows a plot of frequency as a function of acceleration for the above accelerometer. The oscillator circuit used here is discussed in Section 5.4. An 18 volt supply was used and a 0.001 μf capacitor. As shown in Fig. 3-19, the sensitivity is approximately 1.4 KC/g.

3.4 Beam Accelerometers

Another possible mechanical configuration for accelerometers which utilize a needle sensor or indenter point junction combination is a cantilever beam arrangement. A detailed discussion of such an arrangement for use as a force and displacement transducer is given in Section 4.3. The mechanical force in the arrangement discussed in Section 4.3 is simply replaced by a mass under acceleration for accelerometer action. The mass can be the mass of the beam, a mass attached to the beam, or both.

Laboratory accelerometers of the cantilever beam type have been investigated. These devices were found to be extremely fragile and easily broken. The resonant frequency of the cantilever beam accelerometers is low (typically less than 1 KC). The major advantages are its simplicity and range. The beam can be used either to give a mechanical advantage or disadvantage and hence a large range of devices

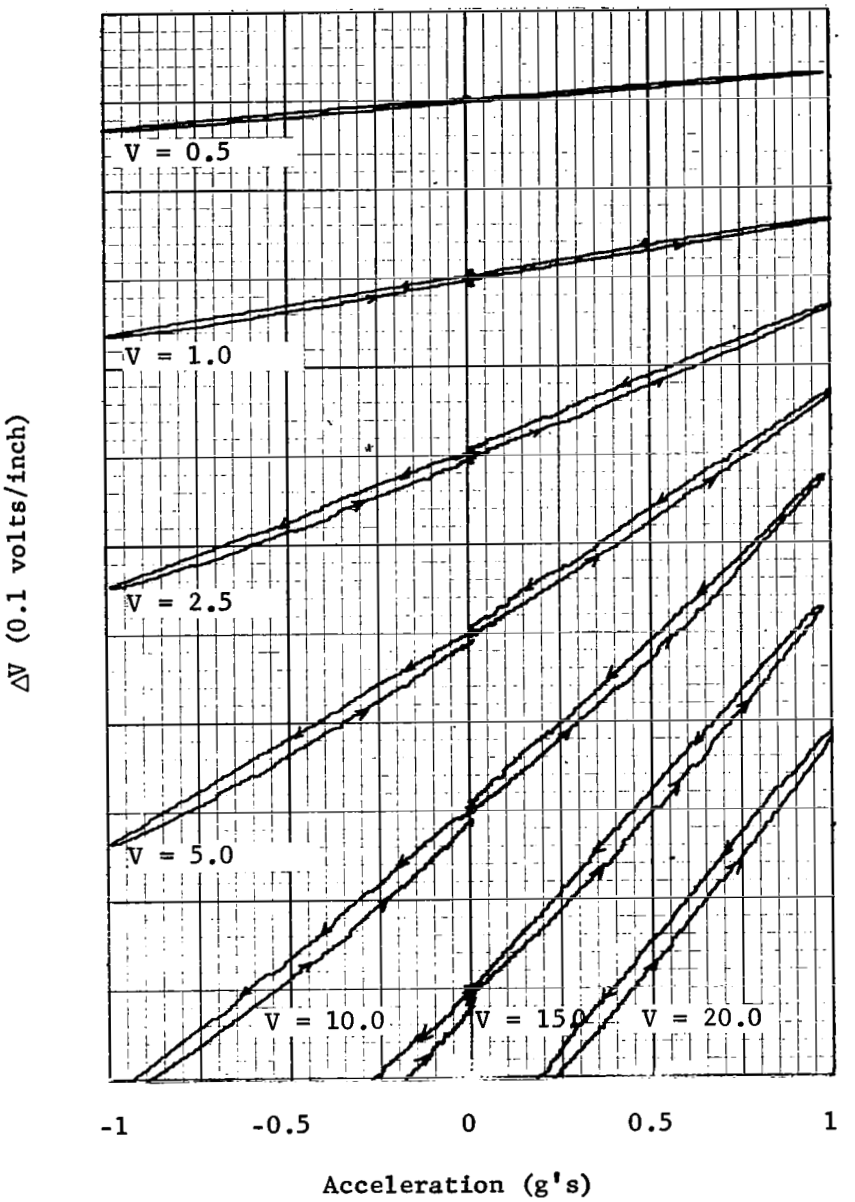

Fig. 3-18. A Recorder Plot of ΔV as a Function of Acceleration for Several Reverse Biased Conditions.

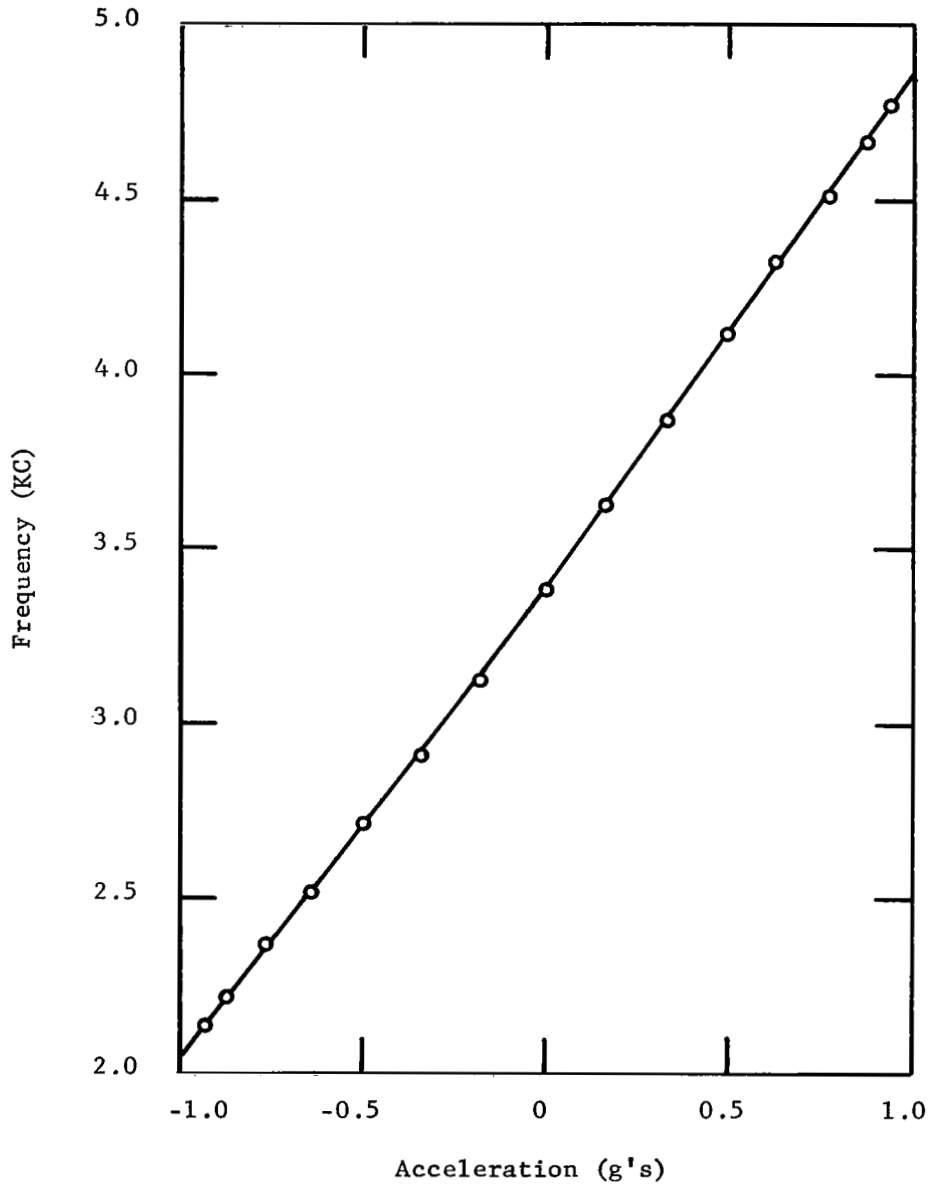

Fig. 3-19. Frequency vs Acceleration for the Accelerometer Shown in Fig. 3-16. The Unijunction Oscillator was Used.

is possible. Low g beam devices are typically sensitive to cross-axis accelerations, however, this can be kept to a minimum by using wide beams.

3.5 Discussion and Summary

Accelerometers of the single-diaphragm, double-diaphragm and beam types have been designed, fabricated and tested. Of the types studied, the double-diaphragm type is definitely the best suited configuration for use with silicon needle sensors. The double-diaphragm accelerometer is, however, the most difficult to construct. As demonstrated by the data presented herein, accelerometers can be fabricated in the range $\pm$ 1 g to $\pm$ 100 g. This does not imply that these are the limiting ranges. In fact, it should be possible to extend both ends by an order of magnitude by choosing the proper radius of curvature for the sensor and the proper mass. Resonant frequency can also be extended by making the bias spring stiffer and reducing the mass both of which are within practical realization.

The major problem with the devices that were tested was the hysteresis effects in the output signal as a function of acceleration. The use of steel pressure plates (bases for the needle) was found to cause large hysteresis effects and non-reproducibility in the characteristics. This was not unexpected since the yield strength of steel is less than the stress levels needed to produce the piezo-junction effect.

The use of silicon as the pressure plate material was found to reduce the hysteresis effect and resulted in reproducible characteristics. An analysis of the data on the accelerometers utilizing the silicon

pressure plates shows that the hysteresis effect is directly related to the sensitivity of the devices. The greater the sensitivity, the greater the hysteresis effect.

Although it is not shown in the data, it was observed that the hysteresis effects were time dependent. The hysteresis loops were found to be smaller when a few minutes were allowed to elapse at each acceleration level. The time required to reach equilibrium was approximately 1 to 2 minutes. As shown by the data, when the acceleration was in the direction of increasing force on the needle, the current was greater on the decending acceleration curve than it was on the ascending portion of the curve. For a negative acceleration, the current was greater when the stress on the needle was being decreased than it was when stress was being increased.

At a first glance, one might suspect that the hysteresis effect is a result of the creation of generation-recombination centers in the junction of the sensor. This model was originally presented as the mechanism responsible for the piezojunction effect. The time dependence is of the correct order of magnitude for such a mechanism. Consider the creation of generation-recombination centers which appear with some very small time constant as stress is applied and which anneal out with a time constant τ after stress is relieved. If τ is much less than the time required to increase and decrease the force on the needle, then there would be no difference observed in the magnitude of the current between an increasing and decreasing force. On the other hand, if τ is equal to or greater than the time required to increase and decrease the force, then a hysteresis effect would be present in

the current-force characteristics. In the latter case, if force were first increased and then decreased, the generation-recombination centers introduced during the force increasing period would remain during the decreasing portion of the cycle and would therefore result in a higher current value. Now if force is decreased and then increased, any generation-recombination centers in the material at the time the cycle is initiated would not have time to anneal out before they were re-introduced, the result being no net change in the current. As shown in the acceleration data in Fig. 3-13, the above conclusions are not observed. In the compression mode the loop closes at zero g and there is a hysteresis present in the stress relieving mode. The creation of generation-recombination centers as a mechanism is therefore ruled out as a cause of the hysteresis. If this mechanism was the cause of the hysteresis then it would be a fundamental limitation on the piezojunction phenomenon.

The observed hysteresis effect is believed to be a result of plastic deformation or non-elastic behavior of the pressure plate material. If the plastic deformation were in the needle it would result in permanent changes in the current or at least generation-recombination centers as discussed above would be created. The contact area between the needle and pressure plate and the stress in the needle would both be affected by plastic deformation or creep effects in the contact region. These effects would result in changes in the current. It would be a formidable task to predict the effect on current since A_s and σ enter into the current relationship in a complex manner, and also the effect of the non-elastic behavior on A_s and σ is not known.

It can be concluded, however, that if a material which is harder than silicon is used as the pressure plate, then any plastic deformation or creep would be limited to the silicon needle. This should result in an increased sensitivity of the needle sensor. Although time did not permit the testing of the hypothesis in accelerometers, it was checked in a force transducer. The silicon pressure plate was replaced by gold plated quartz with the result that the hysteresis effect was eliminated within the measurement capability of the measuring instruments which was on the order of 1%.

Section IV

OTHER TRANSDUCERS

4.1 Introduction

The basic silicon needle sensor can be used as the sensory element in a host of transducer applications. The configurations for employing the silicon needle sensor to measure such parameters as force, displacement and pressure are limited only by the imagination. Several of the more conventional configurations are discussed in the following paragraphs.

4.2 Direct Coupled Force and Displacement Transducer

The simplest method for utilizing the needle sensor to measure force and displacement is the direct coupled device. Here, force is applied directly to the needle. Figure 4-1 shows a sketch of such a device. The spring is used to produce a dc biasing force on the needle sensor. This device consists of a cylinder, a piston, which fits closely into the cylinder, and a rod through which the displacing force is coupled to the piston. The needle sensor is held by the piston so as to receive the applied force.

The relationship between applied force and displacement is given by

$$\Delta X = \frac{FL_r}{E_r A_r} + \frac{FL_p}{E_p A_p} + \Delta y_n \ , \qquad (4.1)$$

where ΔX = Total displacement at end of connecting rod.

F = Displacing force.

E_r, E_p = Moduli of elasticity of connecting rod and piston.

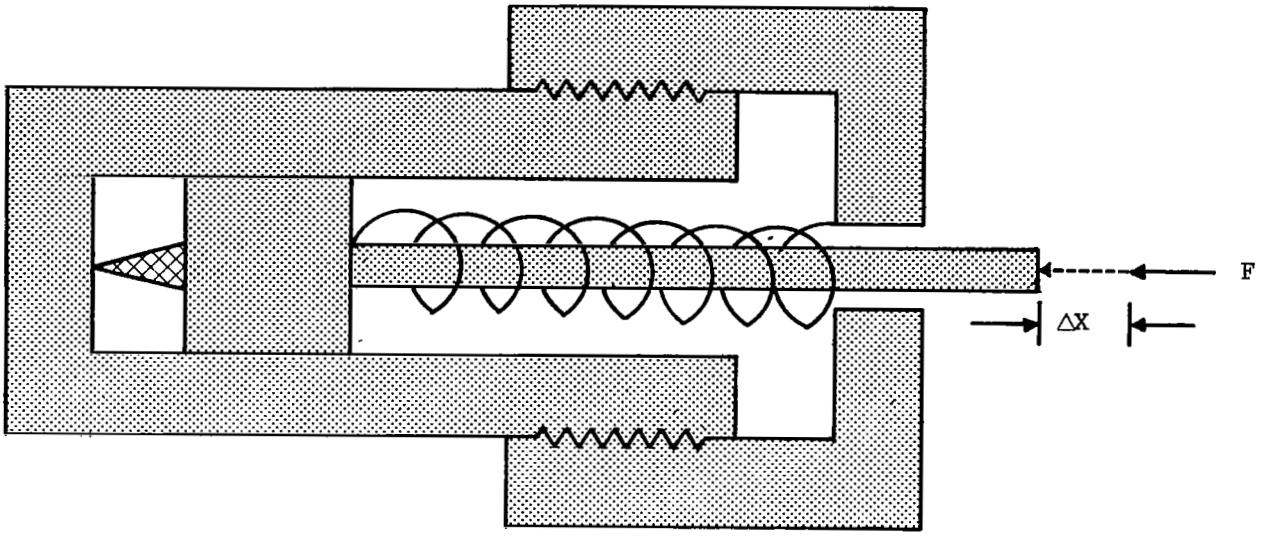

Fig. 4-1. Piston Type Displacement Transducer.

L_r, L_p = Length of rod and piston.

A_r, A_p = Cross-sectional area of rod and piston.

Δy_n = Displacement of needle.

The displacement of the needle is given in Section 2.4.

The disadvantage to this design is the friction in the cylinder. Also, this design is susceptible to shock breakage of the needle.

4.3 Cantilever Transducer

The cantilever beam concept is readily adaptable for use with the silicon needle to measure force and displacement. The basic configuration is shown in Fig. 4-2. If F_a is the applied force on the end of the beam, then the force on the needle (F_n) is

$$F_n = F_a \frac{(3L - a)}{2a} , \qquad (4.2)$$

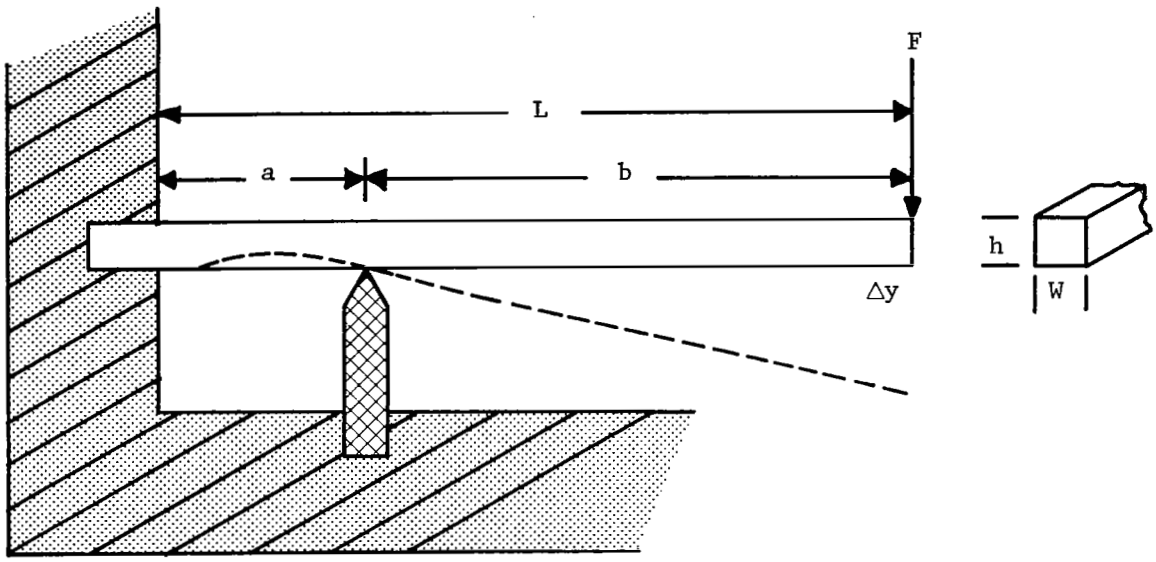

Fig. 4-2. Sketch of Cantilever Beam Force Sensor.

where L is the length of the beam and a is the distance from the cantilever to the needle. The deflection of the end of the beam, Δy, is

$$\Delta y = \frac{4F_a}{EWh^3} (L^3 - (3L - a)^2 a/4) , \qquad (4.3)$$

where E is Young's modulus of the beam, W is the width of the beam, and h is the beam height. Equation (4.3) neglects the compression of the needle. This assumption will be good for thin beams where Δy is in the micron range.

For the case of short thick beams, the compression of the needle must be accounted for. In this case, if Δy_n is the displacement of

the needle, then

$$F_a = \frac{2F_n a - WEh^3 \Delta y_n / 2a^2}{3L - a} , \tag{4.4}$$

The displacement Δy_n is of course a function of F_n as discussed in Section II. The deflection Δy can be solved by combining Eq. (4.4) with the following expression

$$\Delta y = \frac{4F_a L^3}{EWh^3} - \frac{2F_n a^2}{EWh^3} (3L - a) . \tag{4.5}$$

There are several advantages of the cantilever beam over direct coupled needle sensors. As can be seen from Eq. (4.2), there is a mechanical advantage which amplifies the force being measured. Amplifications as high as 10 can be practically realized. Also, the needle position can be interchanged with the force application position to give a mechanical disadvantage. The latter can be mathematically described by simply interchanging F_a with F_n in Eq. (4.2).

A second advantage of the cantilever beam arrangement over direct coupled transducers is its ability to withstand mechanical shock. Shock initiated at the end of the beam is attenuated to some extent before it reaches the needle sensor. Care must be exercised in the design, however, to make sure there is no side motion on the beam.

The practical design of a cantilever beam force transducer requires that the physical dimensions of the beam be considered as well as the needle sensitivity and applied force. As a force transducer, Eq. (4.2) indicates an independence from beam dimensions. There are certain practical limits to an acceptable displacement of the beam.

Also, a practical transducer requires some means for applying a dc biasing force on the needle since a needle sensor requires an approximate stress of 10^9 dynes/cm^2 before the electrical characteristics are altered. One method for applying the dc biasing stress is shown in Fig. 4-3. There are, of course, many other ways to create the dc biasing force.

A typical needle sensor has a force-sensitive range from a threshold of approximately 2 grams to a maximum of 30 grams. As a design example, assume that it is desired to design a cantilever force transducer to measure forces over the range of 0 to 5 grams. As can be seen from Eq. (4.2), a ratio of 1/3 for a/L will give 20 grams on the needle for

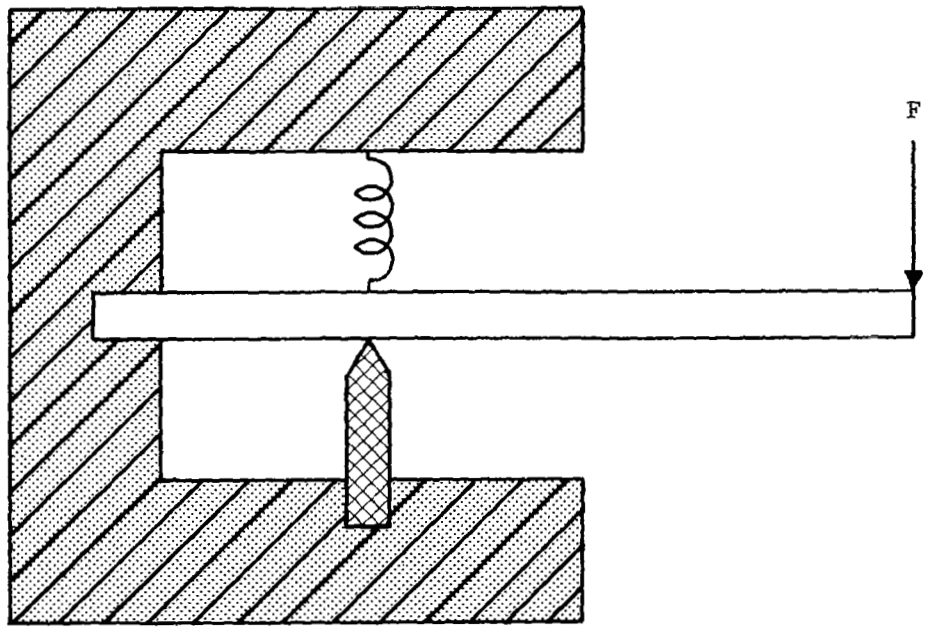

Fig. 4-3. Cantilever Transducer with a dc Biasing Force.

5 grams on the end of the beam. A dc bias load of 5 grams will put the needle in the sensitive range. This will give the needle an operating range of 5 to 25 grams.

As a design example of a cantilever displacement transducer, suppose it is desired to measure displacements over the range 0 to 40 microns. Further, assume that the maximum force that is available without interfering with the system to be measured is 1.5 grams. Consider a stainless steel beam with the following parameters:

$$L = 1/2 \text{ in.}$$

$$W = 1/8 \text{ in.}$$

$$h = .010 \text{ in.}$$

$$a = 0.05 \text{ in.}$$

$$E = 29 \times 10^6 \text{ psi} .$$

From Eq. (4.2),

$$\Delta y = (43.2 \text{ microns/gm}) F_a .$$

A one-gram load will give 43.2 microns in displacement which meets the displacement requirements. The one gram load will result in a force of 30 grams on the needle. The displacement of the needle is negligible in these examples.

4.4 Pressure Sensors

These are basically two methods for fabricating pressure transducers which utilize the piezojunction phenomenon. Both methods utilize a diaphragm to transmit the force to the p-n junction device. The first method utilizes the needle sensor in direct contact with the diaphragm while the second method utilizes a coupling pin between

the diaphragm and the p-n junction device. Both methods are shown schematically in Fig. 4-4.

The diaphragm in these pressure sensors can be made from such materials as stainless steel, quartz or silicon. The latter has proved to be one of the best materials to use in the pressure sensor in which the needle sensor is used.

The deflection at the center of a clamped diaphragm Δy_D under a uniform pressure is

$$\Delta y_D = - \frac{3P\ (m^2 - 1)a^4}{16Em^2t^3} \quad \text{(edges fixed)} , \tag{4.6}$$

where P = Pressure per unit area.

m = reciprocal of Poisson's ratio.

a = radius of diaphragm.

E = Young's modulus of diaphragm.

t = diaphragm thickness.

The deflection at the center of a clamped diaphragm Δy_n under a point load is

$$\Delta y_n = \frac{3F\ (m^2 - 1)a^2}{4\pi Em^2t^3} , \tag{4.7}$$

where F is the point load. The above equations are good for diaphragm deflections less than half the thickness of the diaphragm.

The force on the needle or coupling pin (where the radius of the coupling pin is $\ll$ a) is

$$F = \frac{P\pi a^2}{4} . \tag{4.8}$$

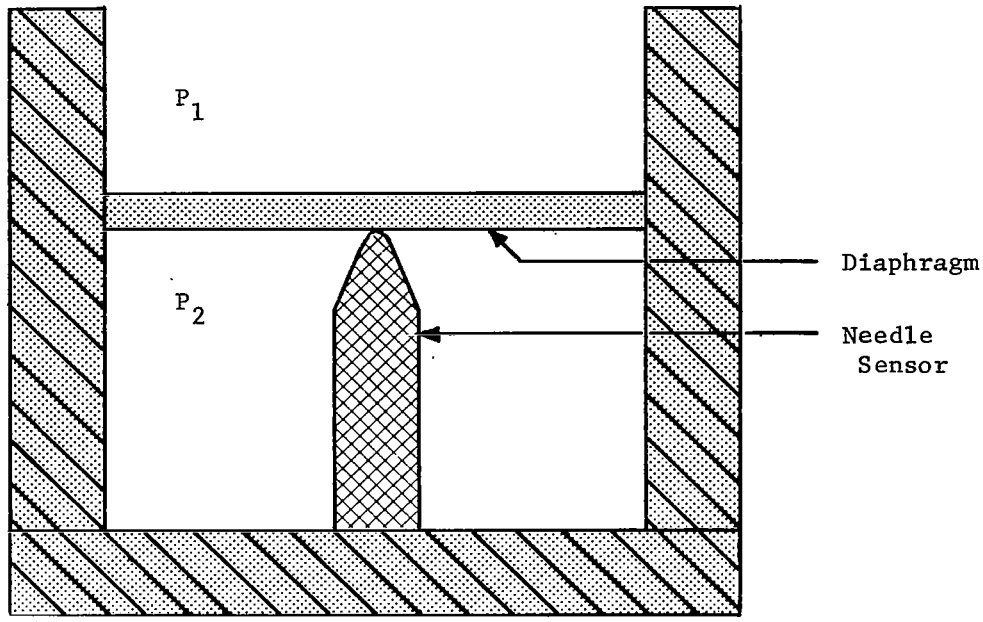

(a) Silicon Needle Pressure Sensor

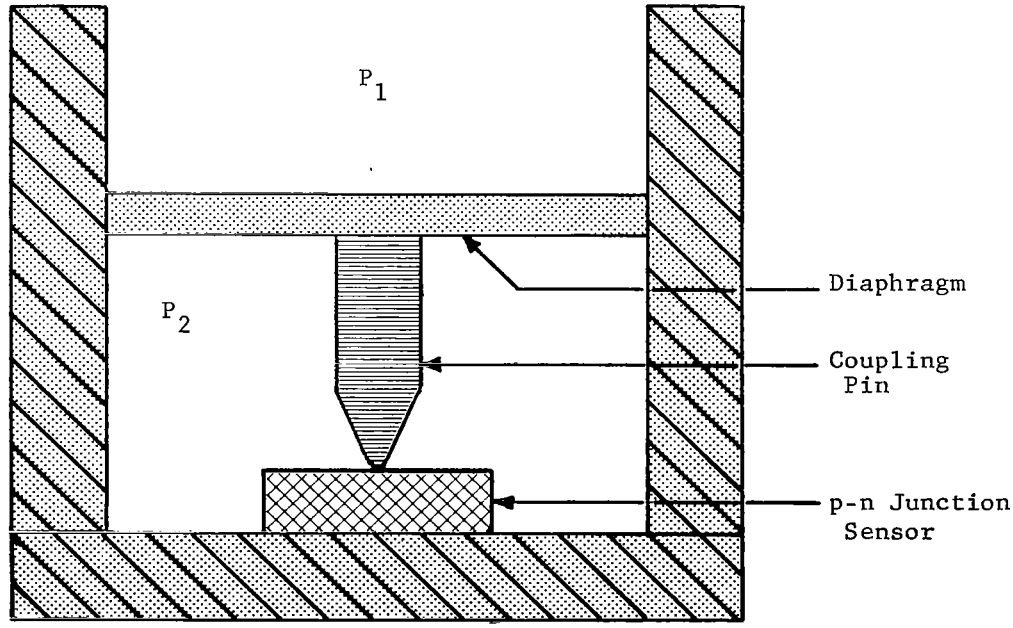

(b) Coupling Pin Pressure Sensor

Fig. 4-4. Piezojunction Pressure Sensors.

If the diaphragm is not too large in radius and is reasonably thick, it can be used to apply the dc bias force needed on the p-n junction sensors. For example, if a stainless steel diaphragm is used with t = 2 mils, a = 0.2 in., a biasing force of 10 grams can be placed on the needle by forcing it against the diaphragm with only an 0.8 mil deflection. In this example, a pressure differential across the diaphragm of 1 psi will apply a force of 14.3 grams on the sensor which is in the proper range for the needle sensor to operate.

Pressure transducers utilizing both the coupling pin and the needle sensor have been fabricated and tested. One of the major advantages of the coupling pin method is that complicated multijunction sensors can be used whereas in needle sensors only one junction is presently available.

A differential pressure transducer of the coupling pin type has been fabricated in which the p-n junction sensor was a four-layer switch. The switch was made using the planar process with a single window as described in Section II.

The transducer consists of a brass housing, a brass diaphragm, inlet and outlet ports, a stainless steel needle, and a planar four-layer switch in chip form. These components were used to form three major assemblies which were then integrated into the final transducer shown schematically in Fig. 4-5.

The diaphragm was cut from 2 mil brass shim stock and fitted to one end of the brass inner housing. The other end of this inner housing was drilled to accommodate an insulated post containing the sensing element and to accommodate the low pressure port. The outer

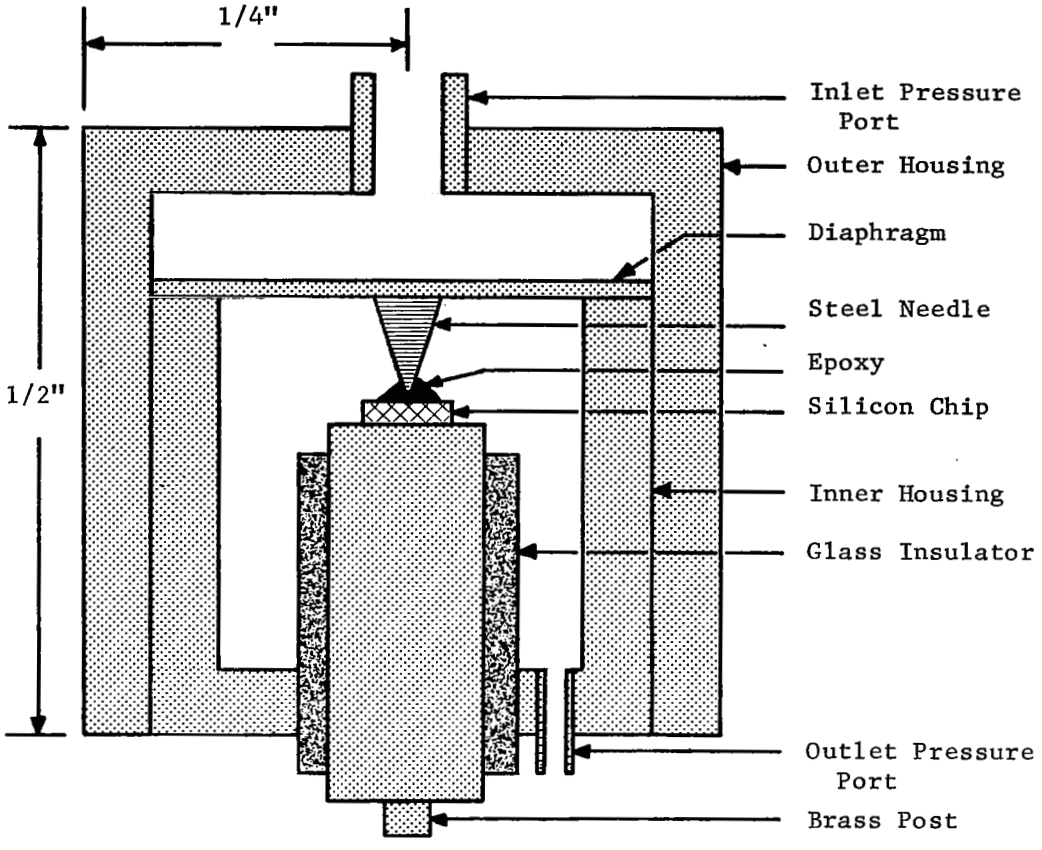

Fig. 4-5. Sketch of Four-Layer Switch Pressure Transducer.

housing was machined so that the inner housing (containing the diaphragm) would fit closely into it. One end of the outer housing was fitted with a brass inlet tube. The brass diaphragm and the inlet and outlet ports were all connected using lead soldering techniques.

The sensing element was made by mounting the chip containing the four-layer switch onto one end of a brass post which was machined to fit closely into a 3/8 inch O.D. glass tube. The chip was held in place by conductive epoxy. The end of the brass post opposite the silicon chip was machined into a terminal for electrical connection.

The purpose of the glass was to electrically insulate the post from the remainder of the transducer.

A steel needle was epoxied to the silicon chip to transmit the force from the diaphragm to the four-layer switch. Armstrong epoxy resin was used.

The first step in the integration of these assemblies was to place the inner housing into the outer housing leaving a small chamber between the inlet port and the diaphragm. The two housings were bonded together by epoxy resin. The sensing element was then placed into the glass insulator and epoxied in place. Conductive epoxy was placed on the bare end of the steel needle and the complete sensing element assembly lowered into the inner cylinder until electrical contact was made between the needle and the diaphragm. Once contact was made, an initial force was produced by lowering the sensing element assembly still further into the inner housing. A photograph of the device is shown in Fig. 4-6 .

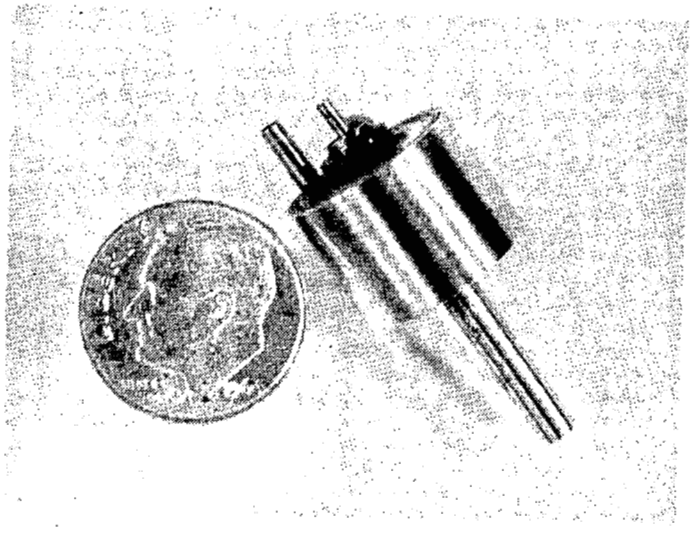

Fig. 4-6. Four-Layer Switch Pressure Transducer.

The completed pressure transducer was calibrated by connecting the four-layer sensing element in a relaxation oscillator circuit (see Section V) and applying a known pressure to the inlet port. The outlet, or low pressure port, was vented to the atmosphere. The center or zero pressure frequency of the oscillator was 91 kc. A frequency change of 20 kc was obtained with a pressure change of 0 to 4 psi. The calibration curve obtained in this manner is shown in Fig. 4-7.

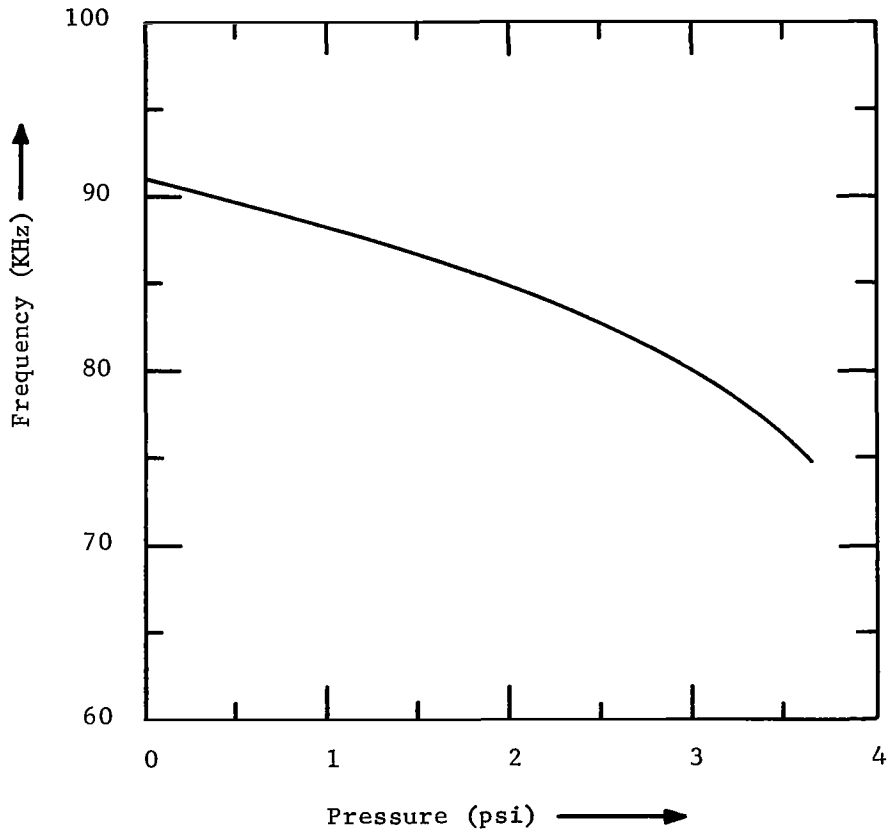

Fig. 4-7. Calibration Curve of Four-Layer Switch Pressure Transducer.

Silicon needle pressure transducers have also been fabricated and tested. These transducers utilized a silicon diaphragm with a thickness of 2.5 mils. The diaphragm was clamped between a rubber O ring and a brass housing. The silicon needle sensor was mounted in a mechanical screw and set in place against one side of the diaphragm. Electrical contact was made by evaporating gold on the silicon diaphragm to which one side of the needle junction made contact. The needle shank was the other contact. The dc biasing force was applied by putting a vacuum on the side of the diaphragm opposite the needle and then setting the needle against the diaphragm by means of the screw. When the vacuum was released, the diaphragm applied the dc bias force. The diameter of the diaphragm was 12 mm. Figure 4-8 is a plot of the sensor current as a function of pressure. The voltage was held constant across the sensor.

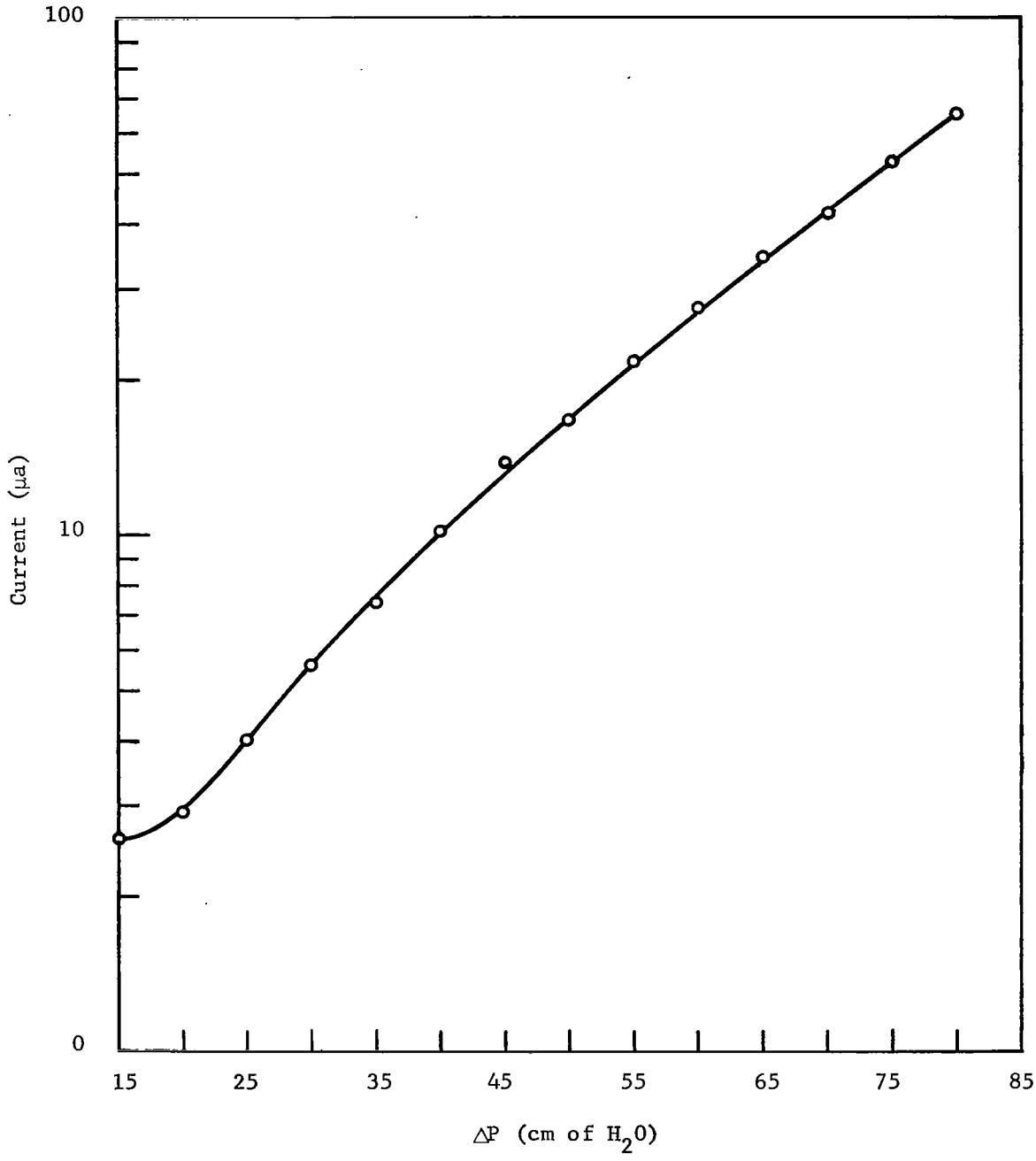

Fig. 4-8. Current in the Reverse Biased Mode as a Function of Pressure for a Silicon Needle Pressure Transducer.

Section V

Read-Out Circuitry for Piezojunction Sensors

5.1 Introduction

Circuitry used in the past for acquiring data from laboratory accelerometers and piezojunction devices was devised specifically for the purpose of evaluating these devices under laboratory conditions. The measuring techniques were conventional and implemented conventional laboratory equipment. The development of accelerometers and other transducers has produced a need for considering circuits which can be used to produce a read-out for the devices in other than laboratory applications. Piezojunction sensors are solid state devices and hence are compatible with microelectronic techniques and devices.

5.2 Differential Amplifier

A simple differential amplifier was devised which produced a 0 - 5V dc output in proportion to a stress input of 5×10^9 to 10^{10} dynes/cm^2 into a p-n junction sensor. Two similar reverse biased diodes were used - one in each leg of the differential amplifier. One diode was the sensing element of an accelerometer and the other was a reference element. The diodes formed a part of a biasing network for the amplifier stages. The zero point is balanced by a variable resistor in the reference stage. A schematic diagram of the amplifier is shown in Fig. 5-1.

5.3 Four-Layer Switch Oscillator

Figure 5-2 is a schematic diagram of a relaxation oscillator in which the frequency is dependent on the input acceleration. The

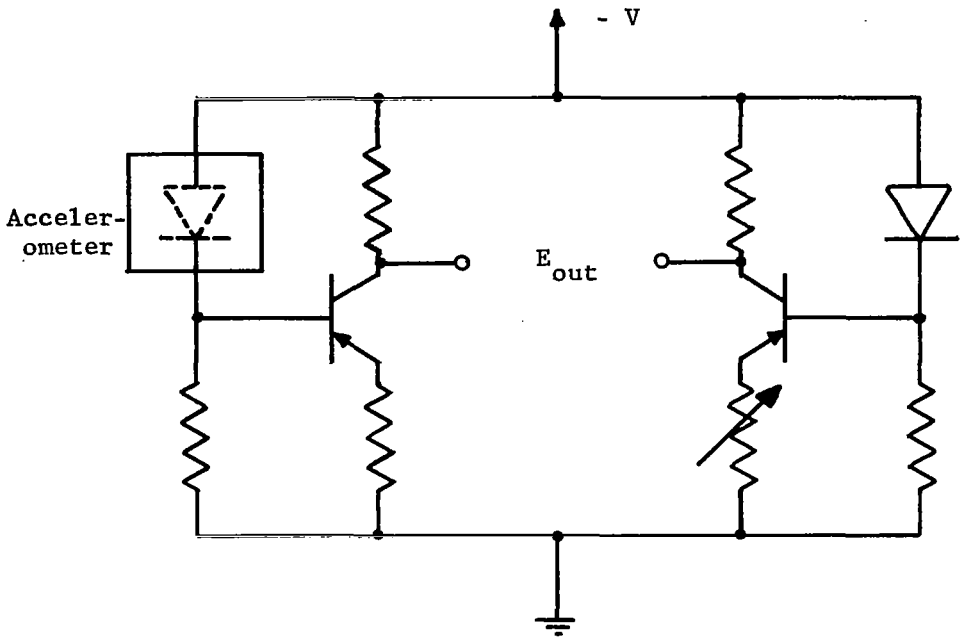

Fig. 5-1. Accelerometer Differential Amplifier.

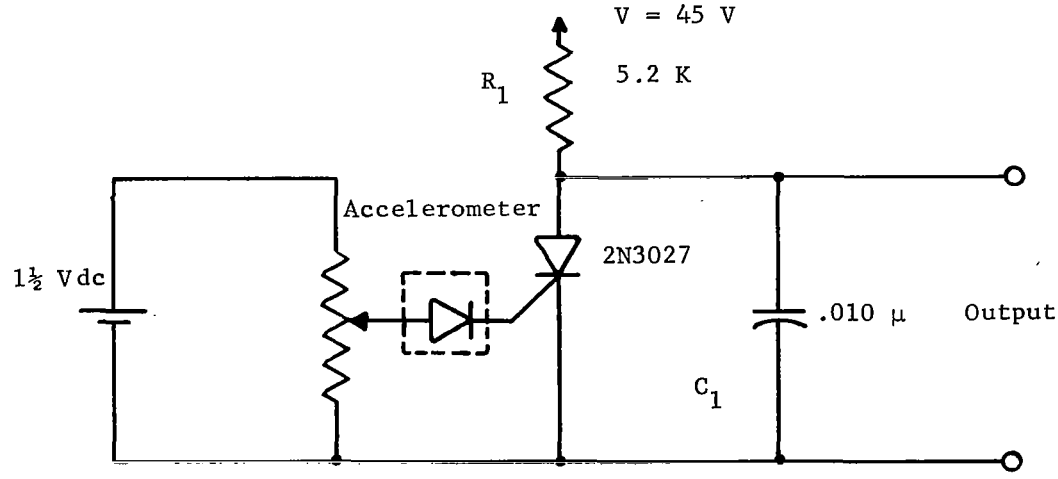

Fig. 5-2. Four-Layer Switch Oscillator Circuit.

active element in the oscillator is a 2N3027 four-layer switching device. The frequency of oscillation depends on the gate current to the device. An accelerometer is placed in series (such that the acceleration sensing junction device is forward biased) with the gate supply. An increase in acceleration allows a rise in gate current and results in an increase in frequency of oscillation. The oscillator frequency is controlled by the R_1C_1 time constant and R of the sensor. Figure 5-3 shows two photographs of the output waveform of the circuit, (a) with no acceleration and (b) under acceleration. A change in both the amplitude and frequency of the waveform can be easily detected in these photographs. However, the change in frequency is the most advantageous measure of input acceleration due to the fact that it can be more easily transmitted without distortion.

The most critical disadvantage of the above circuit has been its instability.

5.4 Unijunction Oscillator

A similar circuit, shown in Fig. 5-4, was designed which utilizes a unijunction transistor as the active element in a relaxation oscillator. The accelerometer acts as an acceleration sensitive resistor in the RC timing circuit of the oscillator. It is this series RC circuit which determines the oscillator frequency. This oscillator is more stable with frequency than the previous circuit. This is partially due to the fact that the frequency of oscillation does not depend directly on a switching level of the unijunction device but is determined by an external circuit. Figure 5-4 is a schematic of the unijunction transistor circuit.

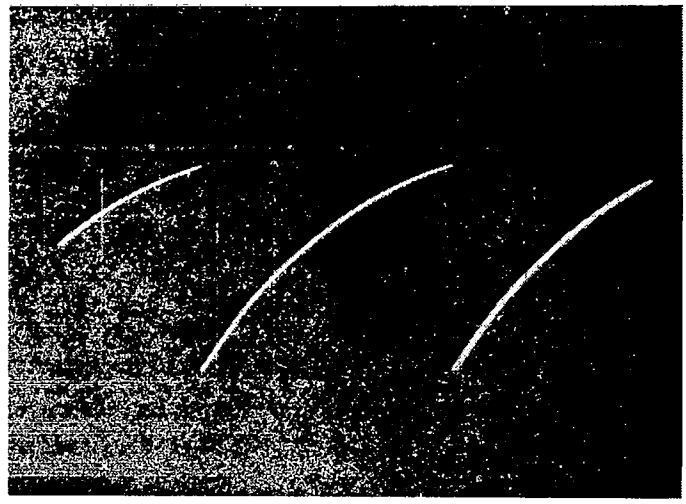

(a) No Acceleration

(b) Under Acceleration

Fig. 5-3. Photographs of Four-Layer Switch Oscillator Waveforms Under Normal and Higher-Than-Normal Accelerations.

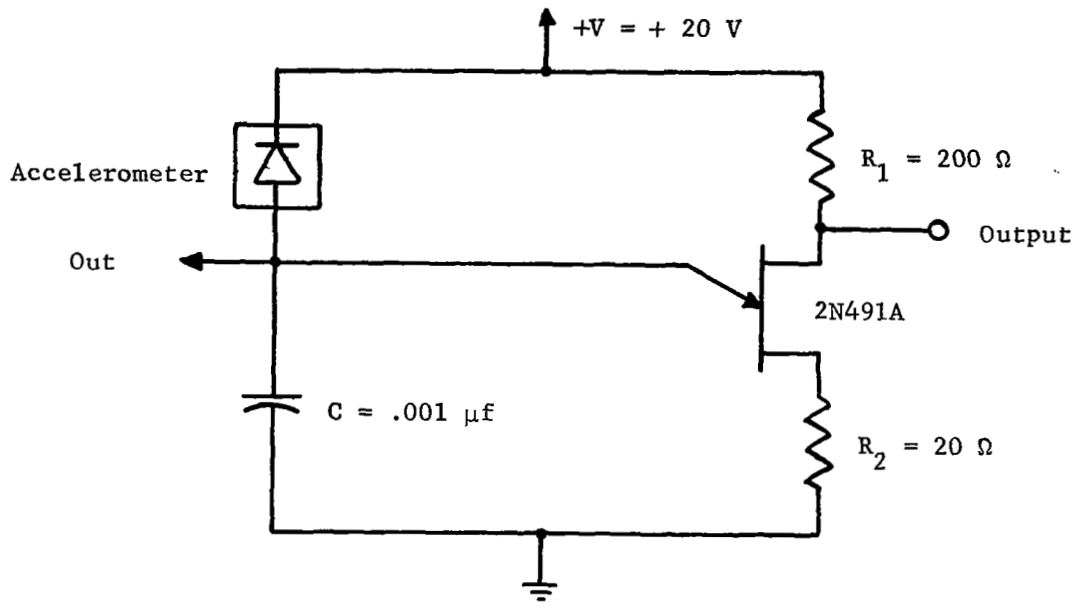

Fig. 5-4. Unijunction Transistor Oscillator Circuit.

5.5 Summary

The circuits described above were developed simply to determine their feasibility and are by no means optimum. There has been no attempt made to environment harden any of the circuits, although the differential amplifier is somewhat inherently temperature compensated. The simplicity of the circuits reflect the lack of difficulty associated with utilizing the piezojunction accelerometers in a practical application. Probably most significant is the ease with which a frequency modulated read-out is obtained.

Section VI

CONCLUSIONS AND RECOMMENDATIONS

This study has shown that mechanical stress applied to the junction area of p-n junction devices can cause large changes in the electrical characteristics of the devices. The underlying mechanism has been found to be a decrease in the effective energy gap of the semiconductor crystal. Analytical expressions have been developed for the effects of stress on the electrical characteristics of diodes, transistors, and four-layer switches. The piezojunction effect showed up in many ways depending on the device configuration and mode of operation. Of the many devices that were studied, the single-junction diode with stress applied to the entire junction area has emerged as one of the best configurations for use in transducer applications.

The silicon needle sensor was conceived and the techniques for fabrication were developed. The needle sensor has the big advantage of not requiring a delicate alignment operation between the stressing arrangement and the junction to be stressed. It also offers the possibility of drastic size reductions in sensors based on the piezojunction effect. One of the problems associated with the application of the needle sensor has been the reduction of the size of the mechanical configurations so that they were not orders of magnitude greater than the sensor size.

A variety of transducers utilizing both the needle sensor and the indenter point method have been investigated. Many of these transducers were fabricated in the laboratory and evaluated. The results of the

study have shown that, in fact, the piezojunction phenomenon can be used as the sensory phenomenon in accelerometers, force, displacement, and pressure transducers. No finalized designs were made, the object here being a study of feasibility of such devices.

Considerable effort has been placed on the demonstration of the usefulness of the piezojunction effect in accelerometers. The double-diaphragm type device was found to be the best configuration studied for use with the needle sensor. These devices showed resonant frequencies greater than 3 KC and are capable of measuring both ac and dc accelerations. Laboratory devices were fabricated with responses covering the range from $\pm$ 1 g to $\pm$ 100 g.

Several techniques were developed for providing a digital output for the piezojunction sensors. The most prominent were the four-layer oscillator and the unijunction oscillator.

There still remains some questions that need to be answered in the application of the piezojunction effect in transducers. One of these is the hysteresis effect as exhibited by the laboratory accelerometers. Although quartz pressure plates appeared to eliminate the effect, it remains to be proven in the accelerometers themselves. Another problem that needs further study is the fragile nature of piezojunction transducers. Methods of preventing overstress and breakage of the sensors need to be investigated. Temperature and long term stability studies of transducers also need to be performed if the devices are to be applied with success and confidence.

The limitations that have been encountered in applying the piezojunction effect in transducers do not appear to be beyond elimination

in practical devices. The phenomenon offers the possibility of a whole new class of transducers that are limited only by one's imagination. The major attributes of transducers based on the piezojunction effect are small size, low power, high sensitivity, high resonant frequency, sensitive to both ac and dc stimuli, and compatibility with micro-electronic circuits and techniques.

LIST OF REFERENCES

[1] J. J. Wortman, "Effect of Mechanical Strain on p-n Junctions", NASA CR-275, August 1965, pp. 1-106.

[2] W. Rindner, "Anisotropic Strain Effects in p-n Junctions", Bull. Am. Phys. Soc. 7, January 1962, pp. 65-66.

[3] M. E. Sikorski, et al., "Transistor Microphone", Rev. Sci. Instr. 33, October 1962, pp. 1130-1131.

[4] W. Rindner, "Resistance of Elastically Deformed Shallow p-n Junctions", J. Appl. Phys. 33, August 1962, pp. 2479-2480.

[5] W. Rinder and I. Braun, "Resistance of Elastically Deformed Shallow p-n Junctions. II.", J. Appl. Phys. 34, July 1963, pp. 1958-1970.

[6] Y. Matukura, Japanese J. Appl. Phys 3, 256 (1964).

[7] T. Imai, M. Uchida, H. Sato, and A. Kobayushi, Japanese J. Appl. Phys. 4, 102 (1965).

[8] J. R. Hauser and J. J. Wortman, "Some Effects of Mechanical Stress on the Breakdown Voltage of p-n Junctions", J. Appl. Phys. 37, No. 10, 3884-3892, September 1966.

[9] J. J. Wortman and J. R. Hauser, "Effect of Mechanical Stress on p-n Junction Device Characteristics. II. Generation-Recombination Current", J. Appl. Phys. 37, No. 9, 3527-3530, August 1966.

[10] W. Rindner, Appl. Phys. Letters 6, 225 (1965).

[11] A. Goetzberger and R. H. Finch, J. Appl. Phys. 35, 1851 (1964).

[12] W. Rindner, G. Doering, and R. Worson, "Structural and Operational Characteristics of Piezotransistors and Applied Devices", Solid State Electronics, Pergamon Press, New York, New York, 1965, p. 232.

[13] W. H. Legat and L. K. Russell, "A Silicon p-n Junction Transducer", paper presented at the 1964 Electron Devices Meeting, Washington, D. C., October 29, 1964.

[14] R. J. Roark, Formulas For Stress and Strain, 9th Ed., McGraw-Hill Book Company, New York, New York (1965).

[15]K. Bulthuis, Phillips Res. Repts., 21, (1966) pp. 85-103.

[16]See Reference Number 5.

[17]S. Timoshenko and J. N. Goodier, Theory of Elasticity, McGraw-Hill Book Company, New York (1951).

[18]H. Hertz, Miscellaneous Papers. Also, Love, Theory of Elasticity, 3rd Ed., Cambridge University Press, (1928).